Title
Melanoma Plasticity Induced by Pro-Inflammatory Cytokines in Response to Immunotherapy

Author
Kim, Yeon Joo

Publication Date
2020

Peer reviewed|Thesis/dissertation

UNIVERSITY OF CALIFORNIA

Los Angeles

Melanoma Plasticity Induced by Pro-Inflammatory Cytokines in Response to Immunotherapy

A dissertation submitted in partial satisfaction of the requirements for the degree Doctor of Philosophy in Molecular and Medical Pharmacology

by

Yeon Joo Kim

2020

ABSTRACT OF THE DISSERTATION

Melanoma Plasticity Induced by Pro-Inflammatory Cytokines in Response to Immunotherapy

by

Yeon Joo Kim

Doctor of Philosophy in Molecular and Medical Pharmacology

University of California, Los Angeles, 2020

Professor Antoni Ribas, Chair

Melanoma dedifferentiation has been reported as a state of cellular resistance to targeted therapy and immunotherapy as cancer cells revert to a more primitive cellular phenotype. In a patient with metastatic melanoma who received adoptive T-cell transfer therapy using T cells with receptors against the melanoma antigen recognized by T cells 1 (MART-1/ Melan-A), we observed dedifferentiation as a resistance mechanism after initial response. However, biopsies obtained from responding patients during anti-programmed cell death receptor 1 (PD-1) therapy had decreased expression of melanocytic markers and increased neural crest markers. When modeling the effects *in vitro*, we documented that melanoma cell lines that were originally melanocytic differentiated underwent a process of neural crest dedifferentiation when continuously exposed to interferon gamma (IFNγ), through a global chromatin landscape change leading to enrichment in specific hyperaccessible chromatin regions. The IFNγ-induced dedifferentiation signature corresponded

with improved outcomes in patients with melanoma, challenging the notion that neural crest dedifferentiation is an adverse phenotype.

The dissertation of Yeon Joo Kim is approved.

Thomas G. Graeber

Stephen T. Smale

Valerie Arboleda

Antoni Ribas, Committee Chair

University of California, Los Angeles

2020

This work is dedicated to my mother, my father, and my brother.

TABLE OF CONTENTS

List of Figures

Chapter 1

Chapter 2

List of Tables

Chapter 1

Acknowledgements

I owe my biggest gratitude to my thesis advisor and mentor Dr. Antoni Ribas. Someone in the lab once told me that I open the office door the way Toni does. That was one of the best compliments I have ever received, because I know that even his smallest actions reflect how caring and mindful he is of others. Toni, I am always humbled by your selfless work ethic and your tireless drive to pursue what will improve the lives of patients. You've taught me that "if I can do more, it is always better to do more," but you've also taught me to develop a discerning viewpoint and be smart with my time. Above everything, your kindness always inspires me and my respect for you is immeasurable. You probably don't know how much everything you did for me meant to me. Doing this PhD was one of the best experiences of my life and I will always be grateful to you for that.

My collaborator Katherine Sheu has done more for this project than I could ever give back. Every time we would meet to talk about science, it reinvigorated me to keep going forward. You are incredibly understanding and intelligent, and I am always awed by your ability to keep center no matter how the rest of the world sways. I am so excited to watch your brilliance continue to unfold in your future.

I would also like to thank all of the members of the Ribas lab, past and present, for everything they do for science. None of my efforts would have been fruitful without your work. There was something for me to learn from every single one of you, whether it be science or life, and I am a better person today because I have met you.

One of the most influential people in my life is my undergraduate PI, Dr. Hanna Mikkola. I remember you pushing me towards the center table on the first day of the Howard Hughes Research Program, not allowing me to waste any second on my hesitation. This perfectly depicts how you mentor me- you always know what I want with more certainty than I do. I hope one day I can be that strong and charismatic rock for others, as you are for me.

The past five years would not have been as full of happiness without Cristina, Giulia, and Gardenia. No words can express how you have enriched my life; my heart swells up just thinking of you. From you I learned how to truly be a friend, how to open up, how to let go, how to stand in other people's shoes, and what it means to be there for someone. I never thought I would ever find people like you that I could call pieces of my soul. You have pulled me through every single difficulty, you have been there every single time I needed help, and you have made every good moment even better. And nothing is more therapeutic than laughing with you for hours!

Most importantly, I would like to thank my world- my mother, my father, and my brother- whom I love more than words could ever describe. My parents instilled in me the love of learning from a very young age. But they have raised me to value family above all, and taught me that the only wealth one should pursue is the wealth of the mind and the soul. I do not know of anyone more thoughtful and selfless, yet resilient and brave, than my parents. I am always humbled and motivated to work harder remembering by how much you have sacrificed for me. And no matter what I achieved in school, you were always there to teach me that what matters more is the depth and the quality of the person I was developing into. Lastly, I am thankful for my younger

brother, who fills all the numerous gaps I leave and plays all these roles for our family that I lack. I am so proud of the wise person you have grown to become and how hard you are working in medical school. You are the best brother I could've asked for and the greatest gift life has given me.

Chapter 1 is a reproduction of the publication with equal contribution to experimental design, data collection, and analysis from Arnav Mehta and Yeon Joo Kim. The study was conceived and supervised by Antoni Ribas.
Mehta, A., Kim, Y. J., Robert, L., Tsoi, J., Comin-Anduix, B., Berent-Maoz, B., ... & Ribas, A. (2018). Immunotherapy resistance by inflammation-induced dedifferentiation. *Cancer discovery*, *8*(8), 935-943.

Chapter 2 was adapted from an article in submission from work that was led by Yeon Joo Kim with contributions from all following authors in experimental design, data collection, and analysis. The study was conceived and supervised by Antoni Ribas.
"Melanoma dedifferentiation induced by interferon-gamma epigenetic remodeling in response to anti-PD-1 therapy" by Yeon Joo Kim, Katherine M. Sheu, Jennifer Tsoi, Gabriel Abril-Rodriguez, Egmidio Medina, Catherine S. Grasso, Davis Y. Torrejon, Ameya S. Champhekar, Kevin Litchfield, Charles Swanton, Daniel E. Speiser, Philip O. Scumpia, Alexander Hoffmann, Thomas G. Graeber, Cristina Puig-Saus, Antoni Ribas.
In submission to *Cell* and *Cancer Cell*, June 2020

Yeon Joo Kim was funded by NIH Ruth L. Kirschstein National Research Service Award F30 CA243248 from the National Cancer Institute.

VITA

EDUCATION

2015-2022	MD/PhD, Medical Scientist Training Program David Geffen School of Medicine at UCLA PhD Candidate (2017-), Department of Molecular and Medical Pharmacology, UCLA
2011-2015	B.S. with Honors in Molecular, Cell, and Developmental Biology, UCLA Regents Scholar (Top 1%)

RESEARCH EXPERIENCE

2017-2020	*Thesis advisor/PI: Dr. Antoni Ribas, UCLA Jonsson Comprehensive Cancer Center, Parker Institute for Cancer Immunotherapy* Interferon-gamma-induced melanoma plasticity and response to anti PD-1 therapy
2016	*PI: Dr. Alex Hoffman, UCLA Institute for Quantitative and Computational Biosciences* Differentiating HOXB4-immortalized hematopoietic stem and progenitor cells into dendritic cells in vitro to test phenotypic and functional equivalence to bone marrow-derived dendritic cells
2015	*PI: Dr. Antoni Ribas, UCLA Jonsson Comprehensive Cancer Center* Genetic engineering of novel chimeric T cell receptors
2011-2015	*PI: Dr. Hanna Mikkola, UCLA Broad Center for Regenerative Medicine* - Integrin alpha-8 selectively marks ectopic cardiomyogenesis from Scl-depleted hemogenic endothelium - Lyve1 distinguishes yolk sac myelo-erythroid progenitor wave from primitive hematopoiesis - c-Met-dependent multipotent labyrinth trophoblast progenitors establish placental exchange interface
2012-2014	*PI: Dr. Fritz C. Eilber, Surgical Oncology, UCLA DGSOM* Effectiveness of neoadjuvant imatinib mesylate treatment of gastrointestinal stromal tumors
2010	*PI: Dr. Michael Schramm, Dept. of Chemistry, Cal State Long Beach* pH Influenced molecular switching with micelle bound cavitands

HONORS AND AWARDS

2020	Keystone Symposium Scholarship
2019	UCLA Pharmacology Department Retreat, Best Poster Award
2019-2022	NIH Ruth L. Kirschstein National Research Service Award F30 (National Cancer Institute) CA243248

2016	Rivenburg Fellowship

PRESENTATIONS

2020	Keystone e-Symposium: Advances in Cancer Immunotherapy (Upcoming), Selected Short Talk Speaker
2020	AACR Annual National Meeting (Upcoming), e-Poster Presenter
2019	UCLA Pharmacology Department Retreat, Poster Presenter
2019	UCLA MSTP Annual Conference, Poster Presenter

PUBLICATIONS

Kim, Y. J., Lek, M. T., & Schramm, M. P. (2011). pH influenced molecular switching with micelle bound cavitands. *Chemical Communications*, *47*(34), 9636-9638.

Ueno, M., Lee, L. K., Chhabra, A., **Kim, Y. J.**, Sasidharan, R., Van Handel, B., ... & Mikkola, H. K. (2013). c-Met-dependent multipotent labyrinth trophoblast progenitors establish placental exchange interface. *Developmental cell*, *27*(4), 373-386.

Lee, L. K., Ghorbanian, Y., Wang, W., Wang, Y., **Kim, Y. J.**, Weissman, I. L., ... & Mikkola, H. K. (2016). LYVE1 marks the divergence of yolk sac definitive hemogenic endothelium from the primitive erythroid lineage. *Cell reports*, *17*(9), 2286-2298.

Grasso, C. S., Giannakis, M., Wells, D. K., Hamada, T., Mu, X. J., Quist, M., ... & Peters, U. (2018). Genetic mechanisms of immune evasion in colorectal cancer. *Cancer discovery*.

Mehta, A., Kim, Y. J., Robert, L., Tsoi, J., Comin-Anduix, B., Berent-Maoz, B., ... & Ribas, A. (2018). Immunotherapy resistance by inflammation-induced dedifferentiation. *Cancer discovery*, *8*(8), 935-943.
(Co-first author)

Grasso, C. S., Tsoi, J., Onyshchenko, M., Abril-Rodriguez, G., Ross-Macdonald, P., Wind-Rotolo, M., … & Ribas, A. (2020). Responses to immune checkpoint blockade therapy through conserved interferon-gamma signaling and decreased immune exclusion. Accepted in *Cancer Cell*.

Kim, Y. J., Sheu, K. M., Tsoi, J., Abril-Rodriguez, G., Medina, E., Grasso, C. S., … & Ribas, A. (2020). Melanoma dedifferentiation induced by interferon-gamma epigenetic remodeling in response to anti-PD-1 therapy. In submission to *Cell* and *Cancer Cell*.

EXTRACURRICULARS AND LEADERSHIP

2019-2020	Student Representative, UCLA Medical and Molecular Pharmacology Department
2017-2020	Member, MSTP Education Committee
2017-2018	MMI Interviewer, UCLA DGSOM MD program Student Interviewer, UCLA MSTP
2016	Anatomy Academy, UCLA DGSOM

Chapter 1

Immunotherapy resistance by inflammation-induced dedifferentiation

[Q1]
[Q2]

RESEARCH BRIEF

Immunotherapy Resistance by Inflammation-Induced Dedifferentiation

Arnav Mehta[1,2], Yeon Joo Kim[1], Lidia Robert[1], Jennifer Tsoi[1], Begoña Comin-Anduix[3,4], Beata Berent-Maoz[1], Alistair J. Cochran[5], James S. Economou[2], Paul C. Tumeh[1], Cristina Puig-Saus[1], and Antoni Ribas[1,4]

ABSTRACT A promising arsenal of targeted and immunotherapy treatments for metastatic melanoma has emerged over the last decade. With these therapies, we now face new mechanisms of tumor-acquired resistance. We report here a patient whose metastatic melanoma underwent dedifferentiation as a resistance mechanism to adoptive T-cell transfer therapy (ACT) to the MART1 antigen, a phenomenon that had been observed only in mouse studies to date. After an initial period of tumor regression, the patient presented in relapse with tumors lacking melanocytic antigens (MART1, gp100) and expressing an inflammation-induced neural crest marker (NGFR). We demonstrate using human melanoma cell lines that this resistance phenotype can be induced *in vitro* by treatment with MART1 T-cell receptor–expressing T cells or with TNFα, and that the phenotype is reversible with withdrawal of inflammatory stimuli. This supports the hypothesis that acquired resistance to cancer immunotherapy can be mediated by inflammation-induced cancer dedifferentiation.

SIGNIFICANCE: We report a patient whose metastatic melanoma underwent inflammation-induced dedifferentiation as a resistance mechanism to ACT to the MART1 antigen. Our results suggest that future melanoma ACT protocols may benefit from the simultaneous targeting of multiple tumor antigens, modulating the inflammatory response, and inhibition of inflammatory dedifferentiation-inducing signals. *Cancer Discov; 8(8); 00–00. ©2018 AACR.*

INTRODUCTION

Despite the high initial response rates of patients to adoptive T-cell transfer therapy (ACT), most patients relapse within a few months (1–3). The prevailing hypotheses for how resistance to ACT develops in patients with melanoma are either that their T cells become ineffective, due to exhaustion or immune tolerance, or that a subset of tumor cells acquire a survival advantage, possibly by genetic alterations that increase proliferation or that result in the loss of presentation of the antigen targeted by ACT (4–9). In recent years, an alternative mechanism, inflammation-induced dedifferentiation of tumor cells to precursor cells of neural crest origin (10–12), has come to light from mouse studies and using human cell lines. Work by Landsberg and colleagues (11) in a mouse model demonstrated that ACT using T cells specific for the shared melanosomal antigen gp100 resulted in initial tumor responses followed by regrowth of cancer cells that had lost gp100 expression and

dedifferentiated into a neural crest lineage. This tumor cell dedifferentiation was mediated by tumor necrosis factor alpha (TNFα) produced by the gp100 T-cell receptor (TCR) transgenic T cells in response to gp100 antigen recognition.

The inflammatory cytokine-induced plasticity of tumor cells, with reversible loss of the tumor-targeting antigen (11, 13), may have widespread clinical implications on how best to target antigens in ACT. Here, we show clinical and pathologic findings from a patient who received MART1-specific ACT and developed resistance to therapy in association with a dedifferentiated tumor phenotype that lacked conventional melanocytic antigens.

RESULTS

Clinical Case Report

A 60-year-old man with multiple pigmented nevi over his body presented with metastatic melanoma and was enrolled in a clinical trial of MART1 TCR-engineered ACT immunotherapy in combination with MART1 peptide-pulsed dendritic cells (DC) and high-dose IL2, administered after a lymphodepleting conditioning regimen (Fig. 1A; NCT00910650). Two years prior, he had noted a mole on his back that had grown and bled occasionally; however, it spontaneously regressed over time. Three months prior to presentation, he noted a right posterior neck mass, and 1 month prior to presentation, he was admitted for abdominal pain and jaundice. Endoscopic retrograde cholangiopancreatography (ERCP) revealed peripancreatic masses, and a fine-needle biopsy raised the possibility of melanoma. A whole-body PET/CT scan revealed multiple metastases in the lungs, head and tail of the pancreas, stomach wall, right lobe of the liver, and peritoneal and mesenteric regions (Fig. 1B). An incisional biopsy of the right posterior neck mass confirmed a MART1-positive metastatic melanoma. HLA typing of the patient revealed HLA-A*0201 positivity, making him a candidate for this clinical trial. This patient was treated before the approvals of immunotherapies that have shown improvement in overall survival in patients with advanced melanoma, such as ipilimumab, nivolumab, and pembrolizumab (14–16).

Per study protocol (Fig. 1A), the patient underwent a nonmyeloablative conditioning regimen of cyclophosphamide (60 mg/kg/day, days −7 and −6) given with mesna (60 mg/kg/day) followed by fludaribine (25 mg/m^2, days −5 to −1). On day 0, the patient received adoptive transfer of 1×10^9 lymphocytes that had been retrovirally transduced with the F5 MART1-specific TCR. On days +1, +14, and +30, the patient received $MART1_{26\text{-}35}$ peptide-pulsed DC vaccines (1.8×10^7, 1.8×10^7, and 1.7×10^7 cells, respectively). Between days +1 and +7, he received high-dose IL2 administered every 8 hours to tolerance. Over the course of the study, peripheral blood was collected at regular intervals for basic laboratory tests and immune monitoring, and he underwent baseline and on-therapy biopsies and PET/CT scans.

At the time of treatment, the patient presented with diffusely metastatic disease confirmed by incisional biopsy of his left neck lesion to be stage IVc melanoma with homogenously positive MART1 (Melan-A) expression by IHC (Fig. 1B). The patient tolerated infusion of F5 TCR T cells, followed by IL2 treatments, and $MART1_{26\text{-}35}$ peptide-pulsed DC vaccines with the main adverse effect being a whole-body skin rash. The patient was able to return to work 1 month after infusion. An early follow-up PET/CT scan at 35 days after infusion demonstrated a dramatic decrease in 2[18F]fluoro-2-deoxy-D-glucose (FDG) uptake in the vast majority of the patient's baseline lesions, with increased uptake in seven lesions and the presence of two new lesions with mild FDG uptake (Fig. 1C; new lesions marked with black arrows and biopsied lesion marked with a red arrow). A subsequent PET/CT scan at 84 days after infusion demonstrated objective responses on most baseline lesions by RECIST. However, there were also several new and increasingly FDG-avid lesions (Fig. 1D; biopsied lesion marked with a red arrow) concerning for progression of disease including on his right anterior chest, liver, and paraspinal, paraaortic, and mesenteric regions, among others. The right anterior chest wall lesion was biopsied at that time for further investigation of his progressing disease. The patient's progression-free survival was 3 months, and his overall survival was 5 months.

Loss of MART1 Antigen in Regressing and Relapsed Tumors

The initial biopsy of the patient's left neck lesion (Fig. 1B, red arrow) showed an atypical malignant epithelioid neoplasm that was consistent with melanoma. IHC staining was performed and showed strong, diffuse S100 and melanocytic antigen expression, including MART1, gp100, and tyrosinase (Fig. 1E). One month after infusion of the F5 TCR T cells, the same left neck lesion was biopsied but showed a heterogeneous pattern of MART1 staining with multifocal areas of low or absent MART1 expression (Fig. 1F). S100 staining showed no difference in intensity and distribution of expression when compared with the initial biopsy; however, gp100 and tyrosinase staining patterns mimicked the multifocal MART1 pattern (Fig. 1F). At the time of progression, an anterior chest lesion biopsy revealed the complete absence of MART1 expression, along with absence of gp100 and tyrosinase, but again a normal S100 staining pattern (Fig. 1G). The global loss of melanocytic antigens, as opposed to just MART1, suggested a phenotype switch (13) within the progressing tumor.

Figure 1. Progressive tumors after ACT demonstrate loss of melanocytic antigens. **A,** Overall treatment course for this patient. The patient was treatment naïve at the time of initiation of the ACT protocol. The patient underwent leukophoresis, and peripheral blood mononuclear cells (PBMC) were used to manufacture T cells for ACT and DCs for use in a $MART1_{26\text{-}35}$–pulsed DC vaccine. The patient underwent nonmyeloablative conditioning with cyclophosphamide and fludarabine started at day −7 prior to ACT. He received the DC vaccine on days +1, +14, and +30 after ACT. Several follow-up PET/CT scans were performed, initially showing disease regression at day +35 and eventual progression by day +84. **B–D,** PET/CT scans of the patient are shown at (**B**) baseline before ACT, (**C**) during tumor regression on day +35 of ACT, and (**D**) during tumor progression on day +84 of ACT. Red arrows indicate biopsied tumors and black arrows indicate progressing lesions at day +35. **E–G,** IHC of the patient's tumor for expression of S100, MART1, CD8, gp100, and tyrosinase at (**E**) baseline before ACT, (**F**) during tumor regression, and (**G**) during tumor progression. A heterogeneous, multifocal loss of MART1 and gp100 is seen during tumor regression, with complete loss of these melanocytic antigens at the time of tumor progression.

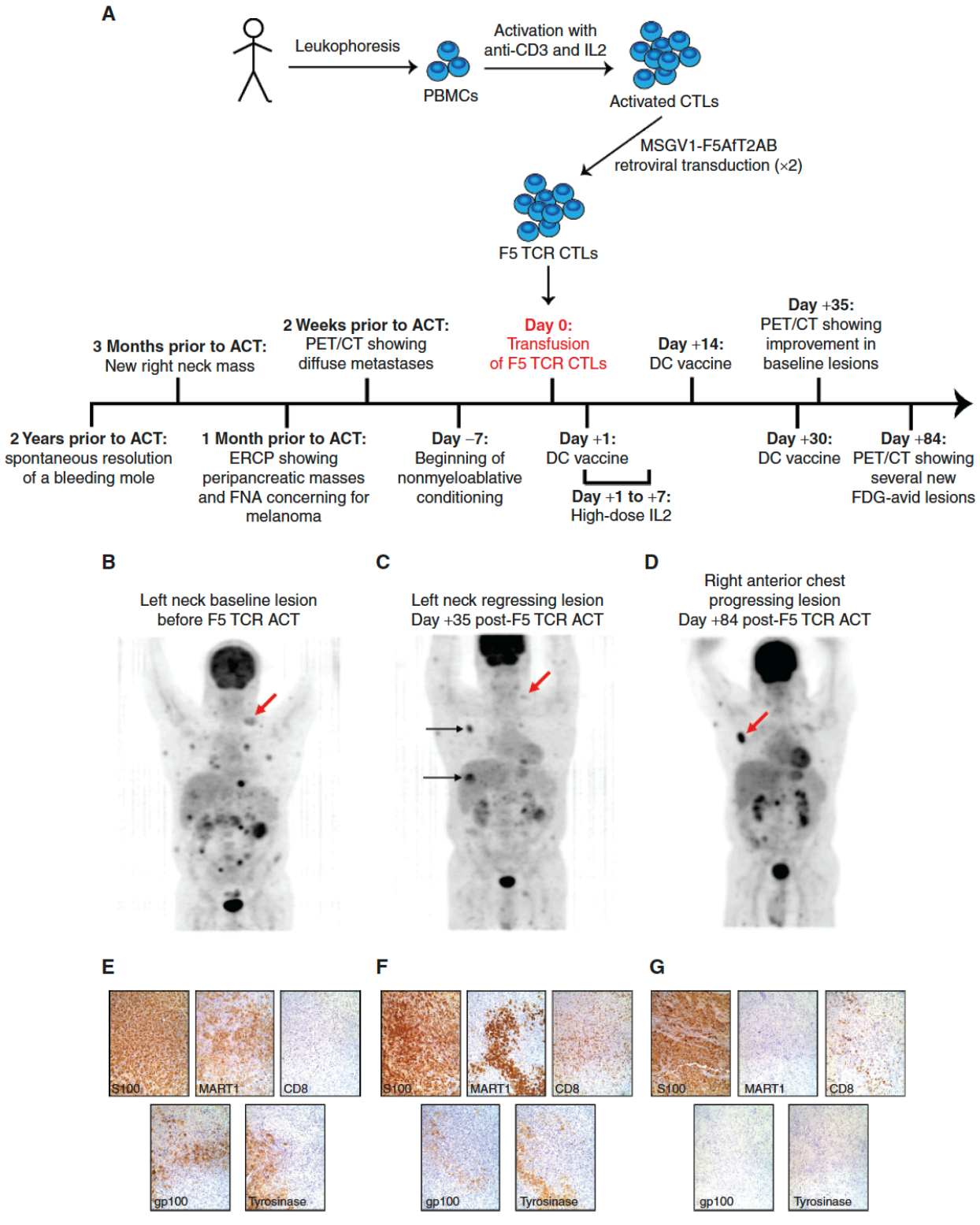
A
Leukophoresis
PBMCs
Activation with anti-CD3 and IL2
Activated CTLs
MSGV1-F5AfT2AB retroviral transduction (×2)
F5 TCR CTLs
2 Years prior to ACT: spontaneous resolution of a bleeding mole
3 Months prior to ACT: New right neck mass
1 Month prior to ACT: ERCP showing peripancreatic masses and FNA concerning for melanoma
2 Weeks prior to ACT: PET/CT showing diffuse metastases
Day −7: Beginning of nonmyeloablative conditioning
Day 0: Transfusion of F5 TCR CTLs
Day +1: DC vaccine
Day +1 to +7: High-dose IL2
Day +14: DC vaccine
Day +30: DC vaccine
Day +35: PET/CT showing improvement in baseline lesions
Day +84: PET/CT showing several new FDG-avid lesions
B
Left neck baseline lesion before F5 TCR ACT
C
Left neck regressing lesion Day +35 post-F5 TCR ACT
D
Right anterior chest progressing lesion Day +84 post-F5 TCR ACT
E
F
G
S100
MART1
CD8
gp100
Tyrosinase

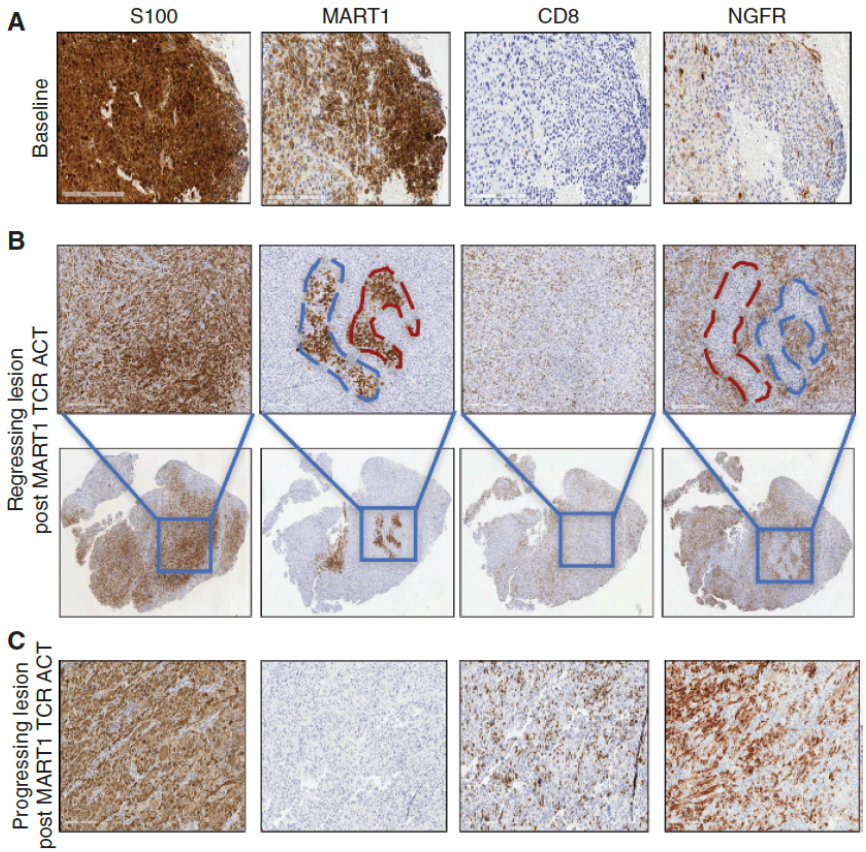

Figure 2. Loss of melanocytic antigens is associated with increased nerve growth factor receptor (NGFR) expression and T-cell infiltration. **A–C,** IHC of the patient's tumor for S100, MART1, CD8, and NGFR (CD271), (**A**) at baseline before ACT, (**B**) during tumor regression, and (**C**) during tumor progression. The loss of MART1 is correlated with higher NGFR expression and CD8 T-cell infiltration in both regressing and progressing tumors, thus suggesting inflammation-induced tumor dedifferentiation of these tumors.

CD8 Cytotoxic T-Lymphocyte Infiltration in MART1-Deficient Tumor

Prior to ACT, the majority of CD8 CTLs were observed at the periphery of the tumor with few CD8 CTLs present in the central regions of the tumor parenchyma (Figs. 1E and 2A). At 35 days after infusion of F5 TCR T cells, a prominent but multifocal lymphocytic infiltrate was observed within the tumor, largely at the periphery with moderate infiltration of the center of the tumor (Figs. 1F and 2B). At the time of relapse, the anterior chest biopsy revealed a predominance of CD8 CTLs diffusely in all areas of the tumor (Figs. 1F and 2C), in direct contrast to the pattern observed on initial biopsy of pretreated tumors. Evidence supports that the presence of CD8 CTLs is indicative of an increased inflammatory milieu within the tumor microenvironment (11).

Expression of an Inflammation-Induced Dedifferentiation Marker in Relapsed Tumor

The nerve growth factor receptor (NGFR or CD271) is a member of the TNF superfamily group of receptors and has been shown to be a marker of cancer stem cells in melanoma (10). The expression of melanocytic antigens, such as MART1 and gp100, is negatively correlated with the expression of NGFR (10). Importantly, inflammatory signals, largely due to TNFα, result in increased expression of NGFR in mouse models of melanoma and human cell lines *in vitro* (11). In this patient, the expression of NGFR was low in pretreated tumor biopsies (Figs. 1E and 2A). However, increased multifocal expression of NGFR was observed in the tumor 35 days after infusion of F5 TCR T cells (Figs. 1F and 2B). Importantly, the expression of NGFR was negatively correlated with expression of MART1 and gp100 within the tumor and was observed predominantly in regions of increased CD8 CTL infiltration, thus suggesting that its expression was linked to regions of the tumor with increased inflammatory mediators (Figs. 1F and 2B). In the progressing tumor this phenomenon was even more apparent, as the vast majority of the tumor cells did not express MART1 and had strong NGFR expression with heavy infiltration of CD8 CTLs (Figs. 1G and 2C).

F5 TCR T Cells Induce Dedifferentiation in Human Melanoma Cell Lines

To determine if F5 TCR-transduced T cells are sufficient to induce dedifferentiation of human melanoma cells *in vitro*, we cultured the human melanoma cell line M397 with conditioned media from the coculture of F5 TCR T cells with M397

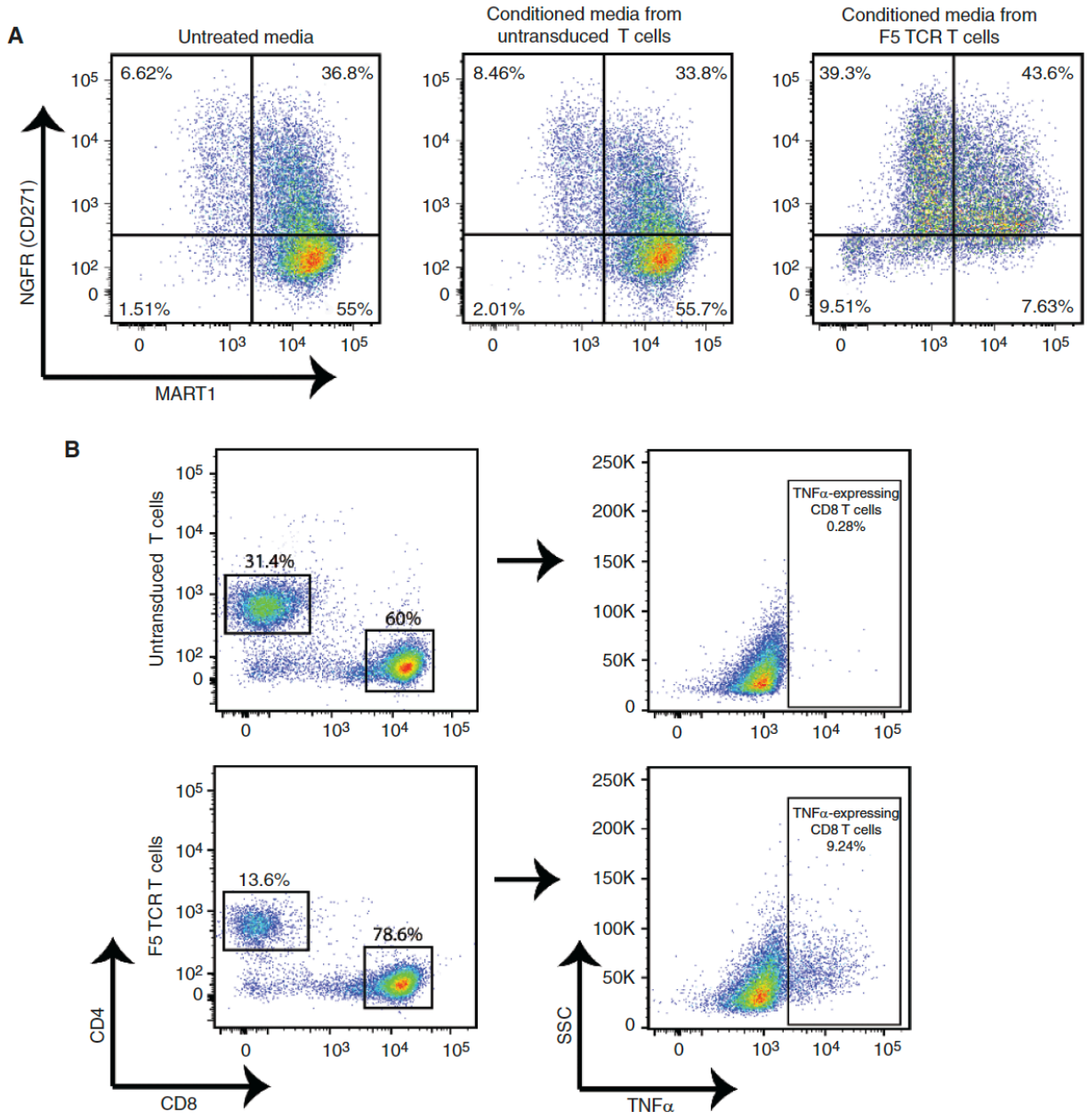

Figure 3. F5 TCR T cells induce dedifferentiation of human melanoma cell lines. **A,** M397 cells were left untreated or cultured for 3 days with conditioned media obtained from coculture of either untransduced or F5 TCR T cells with M397 cells. Flow cytometry was subsequently performed for surface expression of MART1 and NGFR. **B,** Untransduced or F5 TCR T cells were cocultured with M397 cells for 6 hours. Flow cytometry was subsequently performed with intracellular staining for TNFα. SSC, saline sodium citrate.

cells. We were unable to derive cell lines from the patient's biopsy samples; thus, the M397 line was chosen due to its HLA-A2 positivity and expression of MART1. M397 cells cultured with conditioned media generated from coculture with F5 TCR transduced T cells demonstrated decreased surface expression of MART1 and upregulation of NGFR (Fig. 3A). No effect was seen on M397 cells that remained untreated or that were treated with conditioned media from untransduced T cells (Fig. 3A), thus suggesting that conditioned media from F5 TCR T cells are sufficient to induce dedifferentiation of human melanoma cells.

A report in preclinical models had suggested that inflammation-induced dedifferentiation in mouse models of melanoma and in human cell lines is mediated by TNFα (11). To test if F5 TCR T cells produce TNFα upon antigen encounter, we performed intracellular staining of F5 TCR T cells

cocultured with M397 cells and found significantly increased TNFα expression in these cells compared with untransduced cells (Fig. 3B).

TNFα Induces Reversible Dedifferentiation and Markers of ACT Resistance in Human Melanoma

To verify TNFα-induced dedifferentiation in human melanoma cell lines, we treated 8 previously described patient-derived MART1-expressing melanoma cell lines (17) with either TNFα or DMSO for 3 days, and analyzed them for surface expression of MART1 and NGFR (Fig. 4A and B). Consistent with previous findings, we found that TNFα treatment led to dedifferentiation characterized by decreased surface MART1 expression and upregulation of NGFR (Fig. 4A and B). To better understand the molecular mechanism underlying this phenotypic transformation, we performed RNA sequencing of three different melanoma cell lines, M229, M263, and M297, treated with either TNFα or DMSO for 3 days. Gene set enrichment analysis (GSEA) of differentially expressed genes between TNFα- and DMSO-treated cells (Supplementary Tables S1 and S2) revealed that TNFα-treated cells were enriched for genes characteristic of the TNFα inflammatory response [normalized enrichment score (NES) = 2.21, FDR < 0.001], epithelial-to-mesenchymal transition (EMT; NES = 1.92, FDR < 0.001) and neural crest stem cells (NES = 1.49, FDR = 0.016; Fig. 4C). Moreover, genes involved in the microphthalmia-associated transcription factor (MITF) pathway (18), including melanocytic antigens such as MART1, tyrosinase, and PMEL (same as gp100), were enriched in DMSO samples and downregulated in TNFα-treated cells (NES = −2.38, FDR < 0.001; Fig. 4C; Supplementary Table S1). Interestingly, TNFα treatment also led to the enrichment of several pathways characteristic of the innate anti–PD-1 resistance (IPRES) gene signature (ref. 19; Supplementary Table S2). This included enrichment of genes involved in EMT, angiogenesis, and hypoxia, among others (Supplementary Table S2), which is reflective of a more invasive melanoma phenotype and that has been associated with increased NGFR expression (20, 21).

Among the differentially expressed genes with TNFα treatment of our melanoma cell lines were LIF and IL8, both of which are known to promote EMT and tumor resistance (22, 23), thus suggesting that autocrine signaling through these proteins may play a role in tumor dedifferentiation. We thus measured the secretion of IL8 and LIF in the supernatant of M397 cells treated with TNFα or cocultured with untransduced or F5 TCR T cells. Both TNFα and F5 TCR T-cell treatment of M397 cells resulted in increased IL8 and LIF secretion (Supplementary Fig. S1A). However, neither IL8 nor LIF treatment of M397 cells was sufficient to induce dedifferentiation (Supplementary Fig. S1B), thus suggesting that the melanoma resistance phenotype observed in this study is a direct effect of TNFα or may be mediated by factors other than IL8 and LIF.

To test the reversibility of inflammation-induced dedifferentiation in our melanoma cell lines, we treated M397 cells for 3 days with TNFα and subsequently removed the inflammatory media for 7 days (Fig. 4D). Withdrawal of inflammatory media resulted in increased surface MART1 expression and loss of NGFR expression (Fig. 4D), thus suggesting that inflammation-induced dedifferentiation is reversible and that persistent TNFα exposure is required to maintain this phenotypic state.

DISCUSSION

We report a case of melanoma dedifferentiation as a mechanism of immune escape in a patient treated with cancer immunotherapy, a phenomenon previously described only in mouse models and human cell lines (11, 13, 20). The notion of phenotypic switching of melanoma is consistent with our current model of melanoma resistance; that is, we see the loss of the target antigen, in this case MART1, in progressing tumors, which is a phenomenon frequently encountered by pathologists. The global loss of melanocytic markers, including gp100 and tyrosinase, in conjunction with the expression of the inflammation-induced neural crest marker NGFR, suggests that the tumor cells acquired a dedifferentiated state that is reflective of earlier stages of embryologic development of melanocytes, cells that originally arise from within the neural crest. Although it has been suggested that this plasticity of melanoma cells is reversible in mouse models (11), this cannot readily be tested in human patients. Our *in vitro* data using human melanoma cell lines suggest, however, that the same phenomenon may apply to humans, with cells dedifferentiating in the setting of inflammation with the possibility of redifferentiating after inflammation resolves.

Our RNA-sequencing analysis of melanoma cell lines treated with TNFα suggests that the pathways of inflammation-induced dedifferentiation may overlap with those of innate anti–PD-1 resistance (Supplementary Table S2). In particular, the enrichment of genes involved in EMT suggests that dedifferentiation may reflect a more invasive phenotype. This has parallels to resistance patterns observed with BRAF inhibition and may suggest that the concept of phenotypic switching applies more broadly as a resistance mechanism to other modes of melanoma therapy (13, 18, 20, 21, 24, 25). In particular, several hypotheses suggest that the expression of MITF serves as a rheostat for melanoma cell phenotypes, with high levels of MITF promoting differentiation, moderate levels promoting proliferation, and low levels promoting invasiveness (26). MITF is a critical factor for expression of melanocyte pigment genes, and loss of MITF and MART1 (18) with elevated expression of AXL receptor tyrosine kinase and NGFR (20, 21, 27) has been implicated in switching of melanoma cells from a proliferative to an invasive phenotype. Given that invasive cells are more resistant to BRAF inhibition (28), this phenotypic switching may serve as a mechanism to develop resistance to such inhibitors. Single-cell studies of human melanomas at different stages of treatment have revealed that most tumors contain heterogeneous subsets of low and high MITF-expressing cells, with the relative composition of such cells shifting toward low MITF-expressing cells in BRAF or MEK inhibitor–treated patients (27).

This case report suggests that inflammation-induced dedifferentiation of melanoma cells may play a role in evading ACT in a subgroup of patients. In the clinical trial, 13 patients were evaluable for tumor response and 9 patients (69%) showed evidence of tumor regression; however, they all had disease

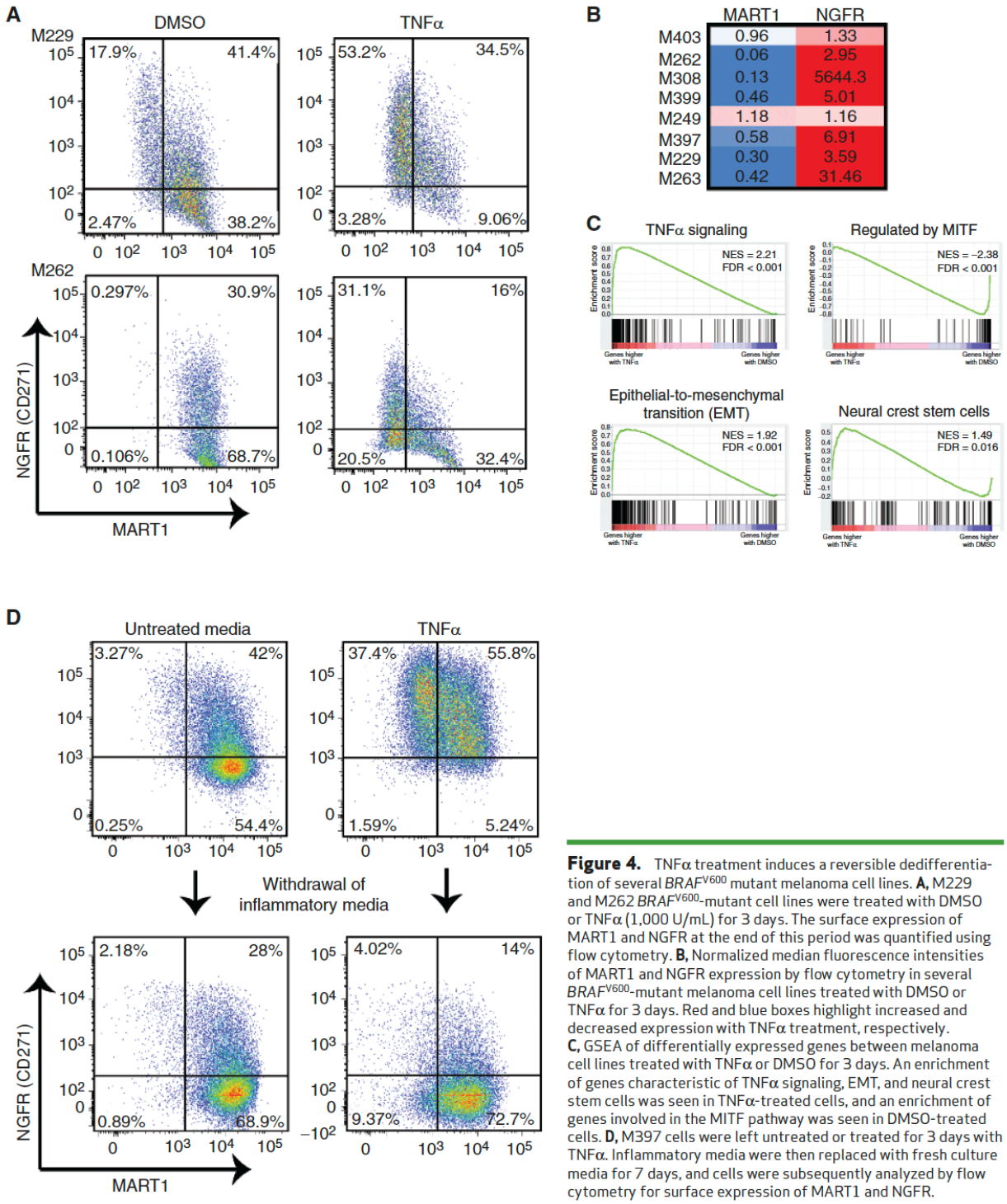

Figure 4. TNFα treatment induces a reversible dedifferentiation of several *BRAF*^{V600} mutant melanoma cell lines. **A,** M229 and M262 *BRAF*^{V600}-mutant cell lines were treated with DMSO or TNFα (1,000 U/mL) for 3 days. The surface expression of MART1 and NGFR at the end of this period was quantified using flow cytometry. **B,** Normalized median fluorescence intensities of MART1 and NGFR expression by flow cytometry in several *BRAF*^{V600}-mutant melanoma cell lines treated with DMSO or TNFα for 3 days. Red and blue boxes highlight increased and decreased expression with TNFα treatment, respectively. **C,** GSEA of differentially expressed genes between melanoma cell lines treated with TNFα or DMSO for 3 days. An enrichment of genes characteristic of TNFα signaling, EMT, and neural crest stem cells was seen in TNFα-treated cells, and an enrichment of genes involved in the MITF pathway was seen in DMSO-treated cells. **D,** M397 cells were left untreated or treated for 3 days with TNFα. Inflammatory media were then replaced with fresh culture media for 7 days, and cells were subsequently analyzed by flow cytometry for surface expression of MART1 and NGFR.

progression within 6 months (29), similar to other TCR-engineered ACT trials (30). There were 4 patients with biopsies at progression, and only this case had evidence of dedifferentiation. This highlights the critical need for more studies investigating the underlying mechanisms of ACT resistance in human patients. These data are important in suggesting that future ACT protocols may benefit from the simultaneous targeting of multiple tumor antigens using mixed T-cell populations and from broadening of the response by concurrent administration of checkpoint inhibitors, so that dedifferentiation and loss of critical melanocytic antigens such as MART1 and gp100 do not contribute

to treatment resistance. In addition, concurrent reduction of the T cell–induced inflammatory milieu that is associated with elevated NGFR expression may also enhance therapeutic efficacy.

METHODS

Study Design

This was a pilot clinical trial for patients with metastatic melanoma (Clinicaltrials.gov number NCT00910650; refs. 31–33). The study protocol and its amendments were approved by the University of California, Los Angeles, Institutional Review Board. The patient provided written informed consent.

Manufacture of Cell Products

The patient underwent leukapharesis to collect peripheral blood mononuclear cells (PBMC). T cells and DCs were manufactured as previously described (31–33). Briefly, PBMCs were activated using anti-CD3 antibodies (OKT3) and IL2 to enrich for T cells and retrovirally infected with the MSGV1-F5AfT2AB vector. Cells were infused fresh. DCs were produced by *ex vivo* differentiation of PBMCs using granulocyte/monocyte colony stimulating factor and IL4 and pulsed with the $MART1_{26-35}$ anchor–modified immunodominant peptide in the HLA-A2.1 allele (29). Full details are provided in the Supplementary Appendix.

Tumor Pathology and IHC

Formalin-fixed paraffin-embedded baseline and on-therapy biopsies were cut and stained with hematoxylin and eosin, anti-S100, anti-Melan-A, anti-CD8, and anti-NGFR antibodies at the UCLA Anatomic Pathology Immunochemistry and Histology Laboratory as previously described (34).

Cell Culture, In Vitro Stimulation, and Flow Cytometry

Human melanoma cell lines were cultured as previously described (17). For *in vitro* dedifferentiation experiments, MART1-specific T cells and untransduced T cells were cocultured with M397 cells, and supernatant was obtained after 24 hours. The conditioned media were diluted 1:1 in fresh culture media for use in subsequent cultures. One million M397 cells were then seeded and treated with TNFα (1,000 IU/mL), conditioned media from MART1 F5 TCR-transduced T cells, conditioned media from mock untransduced T cells, or no treatment for 3 days. To test the reversibility of dedifferentiation, the treatment media were removed from some replicates on day 3 and replaced with fresh culture media for 7 days. All cells were stained with anti-NGFR and anti-MART1 fluorescently conjugated antibodies for analysis by flow cytometry. Intracellular staining was performed using anti-TNFα antibodies after fixation using the Fixation/Permeabilization Solution Kit (BD Biosciences). Samples were analyzed using an LSR-II flow cytometer (BD Biosciences), and the data were analyzed using FlowJo software (TreeStar, Inc.). Full details of all *in vitro* assays are provided in the Supplementary Appendix.

Bulk RNA Sequencing and Analysis

RNA was extracted for three melanoma cell lines treated with either DMSO or TNFα and processed for library preparation. Samples were sequenced by 50-bp single-end sequencing on an Illumina HiSeq 2500 sequencer. Reads were mapped using TopHat2 v2.0.9 (35), and gene expression was quantified using Cufflinks v2.2.1 and Cuffnorm (36). GSEA was used to assess enrichment across several gene sets on the Molecular Signatures Database (MSigDB) and the pathways for IPRES (19). Full details are provided in the Supplementary Appendix.

Disclosure of Potential Conflicts of Interest

No potential conflicts of interest were disclosed.

Authors' Contributions

Conception and design: A. Mehta, Y.J. Kim, P.C. Tumeh, C. Puig-Saus, A. Ribas

Development of methodology: A. Mehta, Y.J. Kim, L. Robert, B. Comin-Anduix, B. Berent-Maoz, A.J. Cochran, P.C. Tumeh, A. Ribas

Acquisition of data (provided animals, acquired and managed patients, provided facilities, etc.): A. Mehta, L. Robert, B. Berent-Maoz, A.J. Cochran, J.S. Economou, P.C. Tumeh, A. Ribas

Analysis and interpretation of data (e.g., statistical analysis, biostatistics, computational analysis): A. Mehta, Y.J. Kim, L. Robert, J. Tsoi, B. Comin-Anduix, A.J. Cochran, P.C. Tumeh, C. Puig-Saus, A. Ribas

Writing, review, and/or revision of the manuscript: A. Mehta, Y.J. Kim, L. Robert, B. Comin-Anduix, A.J. Cochran, P.C. Tumeh, C. Puig-Saus, A. Ribas

Administrative, technical, or material support (i.e., reporting or organizing data, constructing databases): Y.J. Kim, A.J. Cochran, A. Ribas

Study supervision: C. Puig-Saus, A. Ribas

Acknowledgments

This study was funded in part by the UCLA/Caltech Medical Scientist Training Program (to A. Mehta and Y.J. Kim), NIH National Research Service Award CA183220 (to A. Mehta), NIH grants R35 CA197633 and P01 CA168585, the Parker Institute for Cancer Immunotherapy, the Ressler Family Fund, the Samuels Family Fund, the Grimaldi Family Fund, and the Garcia-Corsini Family Fund (to A. Ribas). We would like to thank Nathan Phillips and the UCLA Technology Center for Genomics and Bioinformatics Core Facility for their assistance in processing samples for genomic analysis. We would also like to thank Daniel E. Speiser for his helpful discussions about this work and critical review of our manuscript.

The costs of publication of this article were defrayed in part by the payment of page charges. This article must therefore be hereby marked *advertisement* in accordance with 18 U.S.C. Section 1734 solely to indicate this fact.

Received October 20, 2017; revised May 16, 2018; accepted May 23, 2018; published first June 13, 2018.

Supplementary Material

Immunotherapy resistance by inflammation-induced dedifferentiation

Arnav Mehta, Yeon Joo Kim, Lidia Robert, Jennifer Tsoi, Begoñya Comin-Anduix, Beata Berent-Maoz, Alistair J. Cochran, James S. Economou, Paul C. Tumeh, Cristina Puig-Saus and Antoni Ribas

Supplemental methods

Manufacture of cell products

The patient underwent leukapharesis to collect peripheral blood mononuclear cells (PBMCs). Manufacture of T cells and DCs was started on the day of leukapharesis and was performed as previously described following the investigational new drug (IND) #13859[1-3]. Briefly, 1.5 x 10^9 PBMCs were activated using anti-CD3 antibodies (OKT3) and IL-2 for two days to enrich for T cells and 12 x 10^8 PBMCs were set up for DC culture. T cells were retrovirally infected with the MSGV1-F5AfT2AB (plasmid obtained from Steven A. Rosenberg and colleagues, Surgery Branch, National Cancer Institute) vector on retronectin-coated plates and expanded *ex vivo* for five days. Cells were subsequently placed in infusion bags and infused fresh. DCs were produced in an *ex vivo* differentiation culture containing granulocyte/monocyte colony stimulating factor (GM-CSF) and interleukin-4 (IL-4) for a total of one week. DCs were pulsed with the MART-1_{26-35} anchor-modified immunodominant peptide in the HLA-A2.1 haplotype[4].

Cell lines, cell culture, in vitro stimulation and flow cytometry

Human melanoma cell lines (M series) were established from patient's biopsies under UCLA IRB approval #11–003254. Several human melanoma cell lines, including M229, M263 and M397 were cultured as previously described[5]. Briefly, cells were cultured in RPMI 1640 with L-glutamine (Mediatech,), 10% fetal bovine serum (Omega Scientific), and 1% penicillin-streptomycin (Omega Scientific). Cultures were incubated in a water-saturated incubator at 37°C with 5% CO2. Cell lines were periodically authenticated to their early passages using GenePrint® 10 System (Promega).

For *in vitro* stimulation experiments, cell suspensions from samples treated with DMSO or TNFα (1000U/mL, Peprotech) for 3 days were stained for flow cytometry with fluorescently conjugated extracellular anti-NGFR antibodies (BioLegend). TNF-α was reconstituted in water to 0.5 mg/ml and diluted in 0.1% BSA in PBS to 0.1 mg/ml before applying to cell culture media. After 3 days of treatment, cells were subsequently fixed with Fix-Perm buffer (BD Bioscience) and stained for intracellular MART-1 using a fluorescently conjugated MART-1 antibody (Santa Cruz). Isotypes for mouse IgG1k and mouse IgG1,

respectively, were used to confirm antibody specificity. Live cells were marked with blue live-dead staining (Life technologies) and 10^4 events were collected for each sample. Samples were analyzed using an LSR-II flow cytometer (BD Biosciences) and the data was analyzed using FlowJo software (Tree Star, Inc.).

M397 cell line was chosen for all further cell culture experiments involving T cell co-culture because it is MART-1+, HLA-2.1+, and has been shown to undergo dedifferentation in response to TNFa.

Intracellular staining of PBMCs

M397 cells were seeded overnight in a 24-well plate at 100,000 cells/well. T cells were added at 100,000 cells/well, and BD GolgiPlug and BD GolgiStop (BD Biosciences) were added at 0.5ul/ 1ml and 1ul/ 3ml, respectively, to block extracellular protein transport. Cells were incubated for 6 hours at 37°C before analysis by flow.

Cells were stained using anti-CD45 FITC-conjugated antibody (clone 2D1, BD Biosciences), anti-CD4 BV510-conjugated (clone OKT4), and anti-CD8 BV605-conjugated (clone RPA-T8) antibodies (BioLegend), fixed using Fixation/Permeabilization Solution Kit (BD Biosciences) and stained for intracellular TNFa using anti-TNF PerCPCy5.5-conjugated antibody (clone MAb11, BioLegend).

In vitro dedifferentiation using T cell co-culture conditioned media or recombinant TNFa

PBMCs were isolated by density gradient centrifugation on Ficoll-Paque PLUS (GE Healthcare) from the peripheral blood of a healthy donor. Twenty million PBMCs were activated for 48h in AIM-V media (Thermo Fisher Scientific) supplemented with 5% human AB serum (Omega Scientific), 50 ng/ml anti-CD3 (OKT3, Miltenyi Biotec) and 300 IU/ml rhIL-2 (Proleukin (aldesleukin), Prometheus Laboratories). The cell concentration during this stimulation step was 1×10^6 cells/ml.

MSGV1-F5AfT2AB retrovirus was transduced by 2h centrifugation at 2000g, 32°C on a 6 well tissue culture non-treated plate pre-coated with Retronectin (Clontech).

Activated PBMC were harvested and formulated in AIM-V media supplemented with 5% human AB serum and 300 IU/ml rhIL-2 (0.5×10^6 cells/ml). Two million PBMC were plated per well and centrifuged for 10 min at 1000g, RT followed by overnight incubation (37°C/5%CO2). The above transduction procedure was repeated the next day. After the second transduction round the cells were harvested and kept in culture for at least 96 hours from the time of the first retroviral transduction. Transduction efficiency was tested with MHC tetramer/dextramer analysis for MART-1 (Beckman-Coulter) gated in CD3 (BD Bioscience), CD4 (BD Bioscience) and CD8 (Beckman-Coulter) positive lymphocytes.

The MART-1-specific T cells and untransduced mock T cells were co-cultured with M397 cells in RPMI 1640 with L-glutamine, 10% fetal bovine serum, and 1% penicillin-streptomycin, and the supernatant was obtained after 24 hours. This conditioned media was diluted 1:1 in fresh culture media for use in subsequent cultures.

One million M397 cells were seeded in $10cm^2$ plates overnight and were treated with TNFa (1000IU/ml), conditioned media from MART-1 F5 TCR transduced T cells, conditioned media from mock untransduced T cells, or no treatment for three days. To test reversibility of dedifferentiation, the treatment media was removed from some replicates on day 3 and replaced with fresh culture media for one additional week and analyzed by flow.

ELISA

Cytokines were measured by enzyme-linked immunosorbent assay (ELISA) using TNF alpha human ELISA kit, IL8 human ELISA kit, and LIF human Platinum ELISA kit (Invitrogen) according to manufacterer's instructions. Absorbances were measured using DTX 880 Multimode Detector (Beckman Coulter).

Bulk RNA-sequencing and analysis

RNA extraction of relevant samples was performed using the AllPrep DNA/RNA Mini kit (Qiagen) and libraries were prepared using the TruSeq RNA sample preparation kit (Illumina) per

the manufacturer's instructions. Samples were sequenced using 50bp single-end sequencing on an Illumina HiSeq 2500 platform. Reads were mapped and aligned to the Homo sapiens NCBI build 37.2 reference genome using TopHat2 v2.0.9[6]. Expression values in fragments per kilobase of exon per million fragments mapped (FPKM) were generated using Cufflinks v2.2.1 and Cuffnorm[7]. Gene Set Enrichment Analysis (GSEA) was performed on the transcriptional data using the pre-ranked option with $\log_2$ fold changes as the ranking metric, and averaging over the three different cell lines. Enrichment was assessed across the Molecular Signatures Database (MSigDB) C2 curated gene sets, C6 oncogenic signatures and the previously described signature pathways for IPRES[8].

Supplementary Figures

A

Co-culture treatment	TNFα (pg/mL)	IL8 (pg/mL)	LIF (pg/mL)
Untreated cells	184.24	451.77	620.89
TNFα	23625.54	39527.09	1401.15
Untransduced T cells	179.23	744.20	688.99
F5 TCR T cells	415.58	4224.95	866.99

B

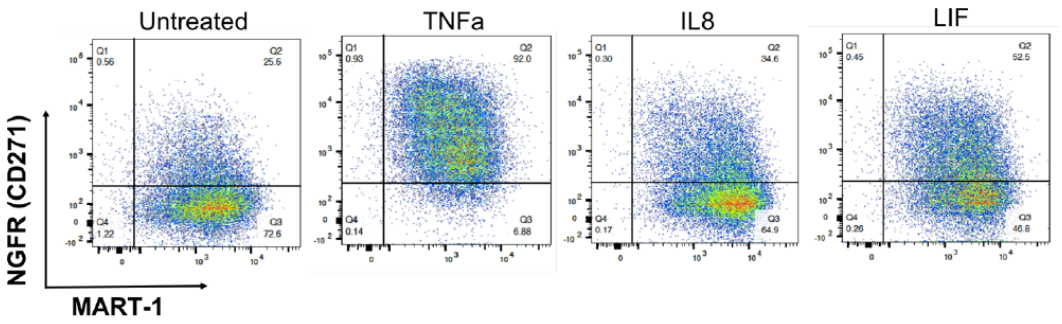

Figure S1. LIF and IL-8 are not sufficient to induce inflammation-induced dedifferentiation of melanoma cell lines. (A) Human M397 melanoma cells were left untreated, treated with TNFα, or with supernatant from co-culture of either F5 TCR T cells or untransduced T cells with M397 cells as described in the supplemental methods. Three days later an ELISA was performed to measure production of TNFα, IL8 and LIF. (B) M397 cells we treated with either TNFα, IL8 or LIF *in vitro* and analyzed by Flow Cytometry at 3 days for markers of dedifferentiation.

Supplementary Tables

Table S1. Gene expression differences between melanoma cell lines treated with either TNFα (1000U/mL) or DMSO for 3 days. The table represents average gene expression in the M229, M263 and M397 cell lines, expressed as the Log_2 value of the fold-change between TNFα and DMSO samples. Listed are all genes that have two-fold higher and two-fold lower expression in TNFα samples compared to DMSO samples.

Genes higher in TNFα samples	Log_2 [fold change (TNFα vs DMSO)]
IL8	7.938465241
CCL2	6.487209082
IL1B	6.186150799
MIR4534	6.140747051
IL32	5.770076954
MIR147B	5.043703627
SNORD49A	5.014272124
MIR4785	4.897520258
SNORD26	4.712761219
C3	4.444247721
UBD	4.416467784
MIR1909	4.248516345
LIF	4.078786291
MIR1182	3.985549716
STC1	3.924839567
TRAF1	3.817454843
MIR3960	3.727973285
SNORD88A	3.4470892
MIR3605	3.395159679
SNORD100	3.384420027
MIR5193	3.367690932
MIR570	3.349784532
IGFBP3	3.346581829
NGFR	3.345208763
TMEM158	3.273288086
INHBA	3.259388959
MIR4690	3.210024108
MIR4517	3.20809683
MMP9	3.194867767
MIR4767	3.181137099
KIAA1199	3.128346079
S100A3	3.038931891
BIRC3	3.003588238
NFKBIA	2.996612363
TNFAIP3	2.995583427
SNORD44	2.977619822
CD70	2.965739297
SNORA77	2.948587465
MMP1	2.942169271
LAMB3	2.931968942
FAM19A3	2.848949316
SNORA17	2.796261766
SNORA78	2.762373262
PODXL	2.750454037
MIR4497	2.690349258
SNORD12	2.688390278
SEMA3B	2.674724732
MIR3975	2.639491895
CTSS	2.637161318
SNORD1C	2.630423329
RELB	2.626642053
LOC100996451	2.620052882
SNORA71B	2.619382575
LRRC15	2.610883201
TFPI2	2.609810455
MT2A	2.609306728
MIR4292	2.602717779
CD82	2.585024677
SNORD23	2.57524668
COL5A3	2.561177289
CLCF1	2.554090088
C1S	2.553583223
SNORD63	2.553284407
MIR24-1	2.553284407
MIR99B	2.540083052
NFKB2	2.50331198
SOD2	2.487740542
SNORD4B	2.475284565
CXCL1	2.463816434
ADAM19	2.453264981
LOC100288866	2.436038218
SNORD82	2.435836831
SNORD6	2.416895625
IL24	2.407473379
AXL	2.405064199
SNORD117	2.399340869
SNORA48	2.377838924
MIR4784	2.363462566
SERTAD4	2.34226453
SNORD50A	2.33666924
SERPINA3	2.31070865
MIR3665	2.307066091
MIR378I	2.299974942
PMEPA1	2.298144572
IER3	2.291900746
IL4I1	2.28209178
RGS16	2.277614945
SNORA13	2.277347834
ICAM1	2.263530842
MIR3190	2.262629834
SNORD48	2.258130023
SNORD24	2.257365597
DEFB124	2.255834752
MIR671	2.237156748
MIR4448	2.235192366
ITGA3	2.234076588
MIR5187	2.22072567
NT5E	2.198538478
STRA6	2.196747827
CD74	2.196496901
AIM2	2.183617416
MIR4258	2.182297125
SNORA46	2.180769165
MIR3164	2.169692742
C10orf10	2.154338884
RNU4-2	2.152847628
MIR3125	2.150753121
CDKN1A	2.148699901
PRKCDBP	2.143863636
IL11	2.135109635
MT1X	2.129703608
ICOSLG	2.127433001
CITED4	2.123820498

PLAUR	2.123273311	CAPS	1.870418425	PLEKHS1	1.672925509
IRAK2	2.12280741	SNORD32A	1.866182624	MATN2	1.667993108
FAM20C	2.113725177	PTX3	1.860300629	SNORA84	1.657789299
MIR3188	2.111508457	FZD1	1.857288705	TAPBP	1.656199729
MIR324	2.10893715	RAC2	1.853588894	ZSWIM4	1.646621794
MIR3916	2.093401447	IRF1	1.843004513	BTBD16	1.645513596
EBI3	2.087824228	MIR4273	1.829946759	GALNTL4	1.640921531
SNORD45A	2.08046866	TPM1	1.825068546	GFPT2	1.638202641
TNFRSF12A	2.0793529	ADAMTS9	1.819721468	OPTN	1.63609797
FN1	2.055619998	LYPD1	1.812664878	ITGB8	1.614748079
KCNN4	2.044462745	RNY4	1.804919317	CHST1	1.613975704
MIRLET7I	2.04167497	MIR4640	1.800919897	MIR4453	1.609476162
SLAMF9	2.03596378	SRGN	1.799414297	OAS2	1.609385987
KYNU	2.029754592	ADAMTS1	1.795433446	IFI27	1.600088861
SQRDL	2.014472251	SNORD12C	1.790114893	MIR137	1.599540281
MIR1224	2.013013222	SAA1	1.782940659	OAS1	1.599175341
DTX4	2.009406011	COL13A1	1.779925559	ACAN	1.596719073
SNURF	2.003463267	MIR221	1.777588404	MDGA1	1.588181864
TMEM132A	1.998370473	JUN	1.776541722	ISG20	1.587657809
SERPINB8	1.992513262	ANXA1	1.774833608	SPRED3	1.58412661
NTM	1.990818758	PLA2G4C	1.771163638	CTHRC1	1.582562621
SERPINB2	1.985966583	ACPL2	1.768976517	MIR937	1.579915627
MIR3651	1.977208777	APOL3	1.768285148	FDCSP	1.573178985
C15orf48	1.974949929	PLAT	1.75338445	IL27RA	1.571062108
CXCL10	1.97285557	RASSF4	1.751055103	SNORA56	1.566482045
MIR4516	1.96262569	VTRNA2-1	1.74604828	JUNB	1.564418073
MIR1178	1.952035587	SNAR-G2	1.734466955	FGFRL1	1.56161911
LCN2	1.951514025	VEGFC	1.731716194	PTGES	1.556728572
CSF1	1.938858121	HLA-DQA1	1.731667289	MIR19B1	1.550737041
CCL20	1.938367283	HDAC9	1.725585065	SNAR-D	1.545960875
MIR126	1.934420208	SNORA5B	1.723436792	EEF1A2	1.545925004
MIR5695	1.934354753	FCRLA	1.715112562	CDC42EP5	1.542420714
ENC1	1.931838461	RNA5SP244	1.712443827	SERTAD4-AS1	1.539453635
SNORD105B	1.927369907	NR4A2	1.711870437	HMGA1	1.536234655
ITGA5	1.92715886	CYB5R2	1.697968732	B4GALNT3	1.534446002
MGLL	1.904878574	REM1	1.692307596	S100A2	1.534281025
MIR3918	1.903193379	S100A16	1.688930395	STX1A	1.531614566
MIR5001	1.8960396	MRGPRX4	1.687847756	PTPRN	1.531394323
NFE2L3	1.890065914	SNORA76	1.686070242	IL1A	1.519050911
BMP2	1.886471282	SNORD68	1.685414495	LOXL2	1.518741883
SNORD116-24	1.879475742	ISG15	1.6790168	GDNF	1.513506181
HLA-B	1.878099248	MRGPRX3	1.677027531	RNU6-35	1.510751537

C1R	1.510492662
SEMA3A	1.507394349
CLDN4	1.502378353
CTXN1	1.500502167
COL18A1	1.497352742
EGR2	1.495291541
GEM	1.491614272
TNIP1	1.486437267
IKBKE	1.486409404
ZNF385A	1.480495212
THBS2	1.479929186
IL34	1.470717594
BCL6	1.470692322
IGFBP7	1.461933875
TM4SF1	1.461532437
PDGFRL	1.457000929
FOSL1	1.455408763
MIR3942	1.446193701
LOC100996570	1.434840167
SLC14A1	1.433660255
ECE1	1.43299577
DCBLD2	1.428099927
DBNDD1	1.425982051
RNU105A	1.424369589
SOX2	1.414414777
WNT5A	1.413034175
CST2	1.412882732
APOL1	1.408202155
CD83	1.405786669
COL6A2	1.405111262
SHISA2	1.402600222
ARHGEF40	1.400883265
SYNGR3	1.394499983
MICALL2	1.394333344
PPM1J	1.392092127
SFRP1	1.383933489
MIR3653	1.380256826
MIR34A	1.380256826
SCARNA27	1.371175851
SLC22A4	1.369473621
FOXC2	1.367405819
IFI6	1.365078044
SEMA4B	1.364652877
ANPEP	1.364626233
PLLP	1.362982624
SERPINE1	1.358489568
TAP1	1.357070075
DDX58	1.355592492
NRP1	1.353704523
FSCN1	1.346480595
SNORA25	1.343720541
RHOC	1.339992538
ANGPTL4	1.33837402
NFKBIE	1.337928923
LOC255130	1.33492042
HMGA2	1.332716379
SNORA2A	1.330368651
ABTB1	1.32876604
BCL3	1.324894541
COL22A1	1.323978557
PSMB9	1.323222428
HIPK2	1.321443168
MYEOV	1.316914195
ADORA2A	1.313953645
SNORD84	1.312673766
TIMP1	1.312549055
GLIPR1	1.312185933
MCL1	1.311764986
PPP1R18	1.311299816
SLC43A2	1.30892543
HLA-H	1.30844061
PHLDA2	1.307017605
OAS3	1.302020382
ANXA2	1.30146261
FJX1	1.300648359
RRAS	1.29484706
FAM108C1	1.290930613
C11orf9	1.29026162
CSRP2	1.279755291
SDC4	1.279069148
WDR54	1.276705114
CAPN5	1.276116033
FADS3	1.271850332
S100A4	1.270337816
RAB13	1.270064375
IFITM1	1.267111491
PALM2-AKAP2	1.266686961
FAM70B	1.264093693
MIR100HG	1.262140526
G0S2	1.258107286
RASAL1	1.253804743
TINAGL1	1.250512414
HSPG2	1.2446909
NARR	1.242686826
NDRG1	1.23921276
NRCAM	1.235019172
LOC100506377	1.231238989
KIAA1549L	1.228412658
ART3	1.224903
C1orf106	1.223363682
SNORA24	1.222856413
SLC2A6	1.220795004
FST	1.215862508
CHST2	1.213898408
CSPG4	1.211815437
KRT7	1.210646866
SYNJ2	1.207686416
S100A6	1.204536097
MAMLD1	1.200834456
SERINC2	1.199185279
COL19A1	1.196655307
PKIG	1.194909346
SNORA5A	1.188765649
PDGFB	1.186412207
TP53I11	1.186127762
ERRFI1	1.185960038
FBN1	1.184605165
GLI2	1.183324048
IL4R	1.181012841
GAS7	1.179860774
PHLDA1	1.179810803
ZMIZ2	1.178541967
PTGS1	1.177417978
USP53	1.177365981
PTPRZ1	1.176225482
LGALS1	1.171766802

SERPINA1	1.16537001
CADM4	1.164326953
HLA-F	1.163804122
AGRN	1.16048784
TNFRSF1B	1.160266968
SMOX	1.159934849
DDR1	1.159313384
IFIH1	1.158852304
SNORA50	1.158115061
RFTN1	1.157072719
SNAR-E	1.156145252
NPTX1	1.156014486
SNORA62	1.154045536
ZYX	1.150797966
ICAM5	1.15037899
NNMT	1.146013564
LOC100128028	1.145785788
AMPD3	1.144927772
SCARNA22	1.142656941
NREP	1.138277211
FLT1	1.13579384
SYNPO	1.134143928
SPARC	1.134020224
TGM2	1.130857498
KIAA0040	1.130846777
ENO2	1.129835247
AFAP1L2	1.125403702
USP11	1.122762022
ETHE1	1.12100603
SLC15A3	1.120883447
SERPINE2	1.12060072
CTSL1	1.119108585
COTL1	1.11777393
CCND1	1.114013186
ARL4C	1.113239352
SYT12	1.109844809
PCDH1	1.108700516
SNORA15	1.108699075
SLAIN1	1.108289764
C1QTNF1	1.106868322
FGFR3	1.105079301
ASPHD1	1.10247142

TRIM8	1.099044216
SLC22A23	1.097731474
GALNT5	1.095500476
IFNGR2	1.092488113
SCARNA16	1.090618455
LTBP2	1.090302655
HAPLN3	1.08771306
IRF7	1.084242077
CNTNAP1	1.08385237
PDLIM4	1.083756577
WTAP	1.082313549
FNDC3B	1.081903257
OCIAD2	1.081156531
SNORA70E	1.080699298
DEPDC7	1.080526319
BST2	1.076928337
NEDD8-MDP1	1.074066039
SNORA1	1.074001806
TIAM2	1.073967591
PREX1	1.07357587
CSRNP1	1.073252993
ROBO4	1.072131276
JAM2	1.071466796
MAP1B	1.070039437
RPPH1	1.06804868
SLC6A6	1.061909101
TSPAN13	1.061210094
GNAI2	1.06113566
SNCG	1.055839179
DNTTIP1	1.053879023
HLA-DQA2	1.053464423
CCL5	1.051693057
SNORA20	1.048505353
SNORA38	1.047815766
SH3PXD2A	1.047171523
OLFML3	1.044666099
LAPTM5	1.042454282
EMILIN1	1.041915267
VASN	1.039882887
HAS3	1.039258194
C16orf45	1.037653985
VWA5A	1.035657976

C5orf45	1.035561171
PLD1	1.034993473
GAS1	1.03463805
SNORD15A	1.032547404
RNF182	1.03210023
SH3BGRL3	1.030851374
SLC5A3	1.028026521
ACOX2	1.025291672
UCP2	1.024493047
BTBD19	1.024297691
PANX2	1.0241392
SEC24D	1.023881317
ITPRIP	1.020943997
TGIF1	1.017675332
ALK	1.017108129
BIK	1.016726784
P4HA2	1.014025008
WFDC3	1.013924652
NUAK1	1.012526053
PPP1R14C	1.009953388
SLC20A1	1.007432836
TIMP3	1.00576372
SEMA6B	1.004954746
MIR3180-4	1.004190534
MMD	1.002852327
LOC100129250	1.002822111
TUBA1A	1.00258016
LOC100507156	1.001033027

Genes lower in TNFα samples	Log_2 [fold change (TNFα vs DMSO)]
ABHD14A-ACY1	-1.001724506
ZNF280A	-1.002214513
HPDL	-1.00612663
BANCR	-1.006661355
RAP2B	-1.006753956
FAM167B	-1.007251133
RHOQ	-1.011505916
BEST1	-1.012050184
LOC115110	-1.012942585
TUBB4A	-1.018385626
CAPN3	-1.01900318
FNIP2	-1.019020457
C21orf91	-1.021154839
SNORA6	-1.02238222
PPIP5K2	-1.02380839
SGK1	-1.024971514
MYO10	-1.0266015
TMEM133	-1.026762514
ACP5	-1.030460078
SNORA70F	-1.035691727
ARHGAP42	-1.038894386
CHAC1	-1.040603746
SNORA7B	-1.043098636
SEMA6A	-1.04456718
H19	-1.044896723
CCL17	-1.046434081
APOLD1	-1.047249027
ATP7A	-1.053419192
ANK2	-1.057942597
P2RX7	-1.058222996
GPM6B	-1.065956207
ABCB5	-1.068664238
SNORA38B	-1.073945626
SNORA70B	-1.075779691
SNORA80B	-1.076364322
SNORA33	-1.088618974
ASNS	-1.089359088
SCARNA20	-1.094428238
NSG1	-1.096803242
NUPR1	-1.100471022
SNORA36A	-1.101626323
SNORA42	-1.101732594
RNASE1	-1.106342914
SNORA30	-1.113747148
BCYRN1	-1.114678405
RNU6ATAC	-1.1170291
HSP90AA6P	-1.117869419
MYEF2	-1.122823201
SETDB2	-1.126819753
RNU4ATAC	-1.128156153
PPP1R3C	-1.128246274
MYO5A	-1.130425838
SWAP70	-1.132159301
RAB27A	-1.138504861
KU-MEL-3	-1.139217273
LOC100128682	-1.140606912
SDCBP	-1.143032133
APOC2	-1.144746864
NAT16	-1.148598962
SNORA28	-1.155181183
LZTS1	-1.155266936
ADCY1	-1.15694587
TRIM48	-1.163705705
SLC19A2	-1.167077969
UBL3	-1.176198341
FAM78A	-1.181528996
MCOLN3	-1.18777348
TNFRSF14	-1.18831067
NBL1	-1.190884817
B3GALT1	-1.202021122
TDRD7	-1.220157778
ATP1A3	-1.220603881
LOC100133445	-1.226591151
SNORD83A	-1.236129322
SNORA22	-1.240049927
LGI3	-1.243045399
MIR5194	-1.243307502
GYG2	-1.250576019
PCDH7	-1.252692042
IGSF11	-1.265724309
PFKFB2	-1.278657183
SNORA34	-1.307919235
MITF	-1.310539448
DNAJA4	-1.312934233
IRF4	-1.328267963
MOB3B	-1.335054101
MIR22	-1.351263023
COMMD3-BMI1	-1.35223783
SNORA41	-1.364552126
PIR	-1.38641808
LGALS3	-1.396558285
CA14	-1.407944923
APOE	-1.408910287
ZFP106	-1.41046911
MIR1231	-1.426489272

SPATS1	-1.427757049
TRPM1	-1.432175759
SLC24A5	-1.433002141
SNORD80	-1.43422124
BCAN	-1.448239316
SNORD8	-1.455219182
RNU6-30	-1.456209561
MIR219-1	-1.465830634
MIR637	-1.468937651
SNAI2	-1.471009291
FAM174B	-1.480617726
LOC100506115	-1.498083763
EEF1E1-MUTED	-1.521000079
MIR663B	-1.525942239
MIR616	-1.542213588
KLF15	-1.560576337
SNORD35B	-1.563188174
TSPAN10	-1.590352851
RAB38	-1.593563874
MIR600	-1.598780549
GDPD5	-1.607664883
SNORA45	-1.614659429
LDB3	-1.621641943
ESRP1	-1.623322749
MIR639	-1.636391019
MIR657	-1.64318635
CHL1	-1.647781047
SPON2	-1.651372734
MIR584	-1.658210087
TRIM63	-1.661872645
MIR4741	-1.662214341
CDK5R1	-1.662587321
TYR	-1.664271092
SNORD116-4	-1.672633215
MIR4763	-1.675785853
MIR659	-1.686624458
SNORD46	-1.701004189
ASAH1	-1.727056838
PMEL	-1.730338789
SNORA3	-1.740701698
SNORD12B	-1.745822838
SNORA7A	-1.749341024

CABLES1	-1.797394417
MIR1304	-1.804592282
PPARGC1A	-1.809465564
RNY3	-1.820737241
MIR4691	-1.845302704
MIR4754	-1.848758015
MIR3176	-1.85984238
MIR135A1	-1.859857465
SNORD124	-1.872805936
MBP	-1.894687355
MIRLET7D	-1.907962964
MIR4523	-1.923912802
MIR4700	-1.926701778
TYRP1	-1.936887279
MIR621	-1.95889018
MIR1273D	-1.965629797
MIR3682	-1.985384751
MIR4665	-1.990843022
MIR4787	-1.991823231
MIR658	-2.01092307
MIR622	-2.012853031
MIR1238	-2.021144637
SNORD11	-2.022246444
MIR1285-1	-2.022246444
STK32A	-2.072609805
MIR4502	-2.112566797
MIR1908	-2.11374264
SNORD14E	-2.11374264
MIR612	-2.134005747
HYPK	-2.164810309
SNORA72	-2.175571949
SCARNA4	-2.221601062
SNORD87	-2.243324717
MIR4312	-2.243324717
SNORD108	-2.245365416
SNORA51	-2.27269813
SNORD66	-2.280657706
GALNT3	-2.290148994
SNORA68	-2.306369313
SLC5A4	-2.333355365
MIR4505	-2.356989622
SNORD5	-2.363487267

MIR4321	-2.44763379
MLANA	-2.461466932
SNORD38A	-2.47678685
SNORD50B	-2.47678685
MIR3187	-2.48973679
SNORD58B	-2.605140575
MIR4458	-2.696190319
SNORD37	-2.714498487
SNORD29	-2.71836449
SNORA52	-2.727094394
SNORD55	-2.734059943
SNORD102	-2.766537
MIR4649	-2.81791162
SNORD15B	-2.846424648
SNORD95	-2.84894296
MIR196A1	-2.852526192
SNORD30	-2.852526192
SNORD54	-2.886289467
MIR941-1	-2.919595182
SNORD75	-3.059763198
DCT	-3.117300277
MIR4737	-3.196433621
MIR922	-3.20851303
SNORA26	-3.27180369
MIR92B	-3.397217592
SNORD34	-3.603988501
MIR1281	-3.642469204
MIR2861	-3.689452343
SNORD14A	-3.91805721
SNORA8	-4.04364241
SNORD35A	-4.174094273
SNORD59A	-4.215425399
SNORA71C	-4.24415629
SNORD65	-5.284151139
SNORD27	-5.308091112
MIR4482-1	-5.551794122
SNORD52	-5.621131615
MIR647	-5.736584765
SNORD96A	-8.094253365

Table S2. GSEA scores across the IPRES signature after 3 days of TNFα (1000U/mL) treatment of several melanoma cell lines, compared to DMSO treatment. Data is from the average gene expression in the M229, M263 and M397 cell lines. NES denotes normalized enrichment score.

IPRES	NES TNF	NOM p-value	FDR q-value
ANASTASSIOU_CANCER_MESENCHYMAL_TRANSITION_SIGNATURE	1.82	0.0001	0.001
VECCHI_GASTRIC_CANCER_ADVANCED_VS_EARLY_UP	1.48	0.001	0.08
MAPKi_INDUCED_EMT	1.81	0.0001	0.0001
LU_TUMOR_ENDOTHELIAL_MARKERS_UP	1.77	0.0001	0.003
LU_TUMOR_VASCULATURE_UP	1.78	0.0001	0.002
ROY_WOUND_BLOOD_VESSEL_UP	1.75	0.0001	0.004
POST_OP_WOUNDHEALING	1.95	0.0001	0.0001
LEF1_UP.V1_UP	1.84	0.0001	0.0001
MAPKi_INDUCED_ANGIOGENESIS	1.77	0.0001	0.0001
EP_BLOOD_VESS_DEVEL_DN_IN_R	2.03	0.0001	0.0001
MISHRA_CARCINOMA_ASSOCIATED_FIBROBLAST_UP	1.7	0.0001	0.008
LIEN_BREAST_CARCINOMA_METAPLASTIC	1.55	0.011	0.047
CHARAFE_BREAST_CANCER_BASAL_VS_MESENCHYMAL_UP	0.96	0.546	0.677
MAHADEVAN_GIST_MORPHOLOGICAL_SWITCH	1.29	0.15	0.224
WESTON_VEGFA_TARGETS_6HR	1.71	0.0001	0.007
WESTON_VEGFA_TARGETS_12HR	1.76	0.0001	0.003
MS_RESP_TO_WOUNDING_UP_IN_MAPKi_aPDL1_NR	1.95	0.0001	0.0001
POOLA_INVASIVE_BREAST_CANCER_UP	1.86	0.0001	0.0001
YE_METASTATIC_LIVER_CANCER	1.34	0.097	0.179
KARAKAS_TGFB1_SIGNALING	1.42	0.064	0.116
JAEGER_METASTASIS_DN	1.41	0.046	0.121
MS_RESP_TO_HYPOXIA_UP_IN_MAPKi_aPDL1_NR	1.68	0.0001	0.0001
LU_TUMOR_ANGIOGENESIS_UP	1.77	0.002	0.002
MAINA_VHL_TARGETS_DN	1.49	0.023	0.075
HARRIS_HYPOXIA	2.04	0.0001	0.0001
JEON_SMAD6_TARGETS_UP	1.88	0.0001	0.0001

REFERENCES

1. Johnson LA, Morgan RA, Dudley ME, Cassard L, Yang JC, Hughes MS, et al. Gene therapy with human and mouse T-cell receptors mediates cancer regression and targets normal tissues expressing cognate antigen. Blood 2009;114:535–46.
2. Robbins PF, Morgan RA, Feldman SA, Yang JC, Sherry RM, Dudley ME, et al. Tumor regression in patients with metastatic synovial cell sarcoma and melanoma using genetically engineered lymphocytes reactive with NY-ESO-1. J Clin Oncol 2011;29:917–24.
3. Morgan RA, Dudley ME, Wunderlich JR, Hughes MS, Yang JC, Sherry RM, et al. Cancer regression in patients after transfer of genetically engineered lymphocytes. Science 2006;314:126–9.
4. Dunn GP, Bruce AT, Ikeda H, Old LJ, Schreiber RD. Cancer immunoediting: from immunosurveillance to tumor escape. Nat Immunol 2002;3:991–8.
5. Khong HT, Restifo NP. Natural selection of tumor variants in the generation of "tumor escape" phenotypes. Nat Immunol 2002;3:999–1005.
6. Khong HT, Wang QJ, Rosenberg SA. Identification of multiple antigens recognized by tumor-infiltrating lymphocytes from a single patient: tumor escape by antigen loss and loss of MHC expression. J Immunother 2004;27:184–90.
7. Taube JM, Anders RA, Young GD, Xu H, Sharma R, McMiller TL, et al. Colocalization of inflammatory response with B7-h1 expression in human melanocytic lesions supports an adaptive resistance mechanism of immune escape. Sci Transl Med 2012;4:127ra137.
8. del Campo AB, Kyte JA, Carretero J, Zinchencko S, Mendez R, Gonzalez-Aseguinolaza G, et al. Immune escape of cancer cells with beta2-microglobulin loss over the course of metastatic melanoma. Int J Cancer 2014;134:102–13.
9. Sharma P, Hu-Lieskovan S, Wargo JA, Ribas A. Primary, adaptive, and acquired resistance to cancer immunotherapy. Cell 2017;168:707–23.
10. Boiko AD, Razorenova OV, van de Rijn M, Swetter SM, Johnson DL, Ly DP, et al. Human melanoma-initiating cells express neural crest nerve growth factor receptor CD271. Nature 2010;466:133–7.
11. Landsberg J, Kohlmeyer J, Renn M, Bald T, Rogava M, Cron M, et al. Melanomas resist T-cell therapy through inflammation-induced reversible dedifferentiation. Nature 2012;490:412–6.
12. Holzel M, Tuting T. Inflammation-induced plasticity in melanoma therapy and metastasis. Trends Immunol 2016;37:364–74.
13. Kemper K, de Goeje PL, Peeper DS, van Amerongen R. Phenotype switching: tumor cell plasticity as a resistance mechanism and target for therapy. Cancer Res 2014;74:5937–41.
14. Hodi FS, O'Day SJ, McDermott DF, Weber RW, Sosman JA, Haanen JB, et al. Improved survival with ipilimumab in patients with metastatic melanoma. N Engl J Med 2010;363:711–23.
15. Robert C, Long GV, Brady B, Dutriaux C, Maio M, Mortier L, et al. Nivolumab in previously untreated melanoma without BRAF mutation. N Engl J Med 2015;372:320–30.
16. Robert C, Schachter J, Long GV, Arance A, Grob JJ, Mortier L, et al. Pembrolizumab versus ipilimumab in advanced melanoma. N Engl J Med 2015;372:2521–32.
17. Wong DJ, Robert L, Atefi MS, Lassen A, Avarappatt G, Cerniglia M, et al. Antitumor activity of the ERK inhibitor SCH772984 [corrected] against BRAF mutant, NRAS mutant and wild-type melanoma. Mol Cancer 2014;13:194.
18. Hoek KS, Eichhoff OM, Schlegel NC, Dobbeling U, Kobert N, Schaerer L, et al. In vivo switching of human melanoma cells between proliferative and invasive states. Cancer Res 2008;68:650–6.
19. Hugo W, Zaretsky JM, Sun L, Song C, Moreno BH, Hu-Lieskovan S, et al. Genomic and transcriptomic features of response to anti-PD-1 therapy in metastatic melanoma. Cell 2017;168:542.
20. Muller J, Krijgsman O, Tsoi J, Robert L, Hugo W, Song C, et al. Low MITF/AXL ratio predicts early resistance to multiple targeted drugs in melanoma. Nat Commun 2014;5:5712.
21. Shaffer SM, Dunagin MC, Torborg SR, Torre EA, Emert B, Krepler C, et al. Rare cell variability and drug-induced reprogramming as a mode of cancer drug resistance. Nature 2017;546:431–5.
22. David JM, Dominguez C, Hamilton DH, Palena C. The IL-8/IL-8R axis: a double agent in tumor immune resistance. Vaccines 2016;4. pii: E22. doi: 10.3390/vaccines4030022.
23. Penuelas S, Anido J, Prieto-Sanchez RM, Folch G, Barba I, Cuartas I, et al. TGF-beta increases glioma-initiating cell self-renewal through the induction of LIF in human glioblastoma. Cancer Cell 2009;15:315–27.
24. Su Y, Wei W, Robert L, Xue M, Tsoi J, Garcia-Diaz A, et al. Single-cell analysis resolves the cell state transition and signaling dynamics associated with melanoma drug-induced resistance. Proc Natl Acad Sci U S A 2017;114:13679–84.
25. Eichhoff OM, Zipser MC, Xu M, Weeraratna AT, Mihic D, Dummer R, et al. The immunohistochemistry of invasive and proliferative phenotype switching in melanoma: a case report. Melanoma Res 2010;20:349–55.
26. Johannessen CM, Johnson LA, Piccioni F, Townes A, Frederick DT, Donahue MK, et al. A melanocyte lineage program confers resistance to MAP kinase pathway inhibition. Nature 2013;504:138–42.
27. Tirosh I, Izar B, Prakadan SM, Wadsworth MH 2nd, Treacy D, Trombetta JJ, et al. Dissecting the multicellular ecosystem of metastatic melanoma by single-cell RNA-seq. Science 2016;352:189–96.
28. O'Connell MP, Marchbank K, Webster MR, Valiga AA, Kaur A, Vultur A, et al. Hypoxia induces phenotypic plasticity and therapy resistance in melanoma via the tyrosine kinase receptors ROR1 and ROR2. Cancer Discov 2013;3:1378–93.
29. Chodon T, Comin-Anduix B, Chmielowski B, Koya RC, Wu Z, Auerbach M, et al. Adoptive transfer of MART-1 T-cell receptor transgenic lymphocytes and dendritic cell vaccination in patients with metastatic melanoma. Clin Cancer Res 2014;20:2457–65.
30. Rosenberg SA. CCR 20th Anniversary Commentary: autologous T cells-the ultimate personalized drug for the immunotherapy of human cancer. Clin Cancer Res 2015;21:5409–11.
31. Ayyoub M, Zippelius A, Pittet MJ, Rimoldi D, Valmori D, Cerottini JC, et al. Activation of human melanoma reactive $CD8^+$ T cells by vaccination with an immunogenic peptide analog derived from Melan-A/melanoma antigen recognized by T cells-1. Clin Cancer Res 2003;9:669–77.
32. Butterfield LH, Ribas A, Dissette VB, Amarnani SN, Vu HT, Oseguera D, et al. Determinant spreading associated with clinical response in dendritic cell-based immunotherapy for malignant melanoma. Clin Cancer Res 2003;9:998–1008.
33. Ribas A, Glaspy JA, Lee Y, Dissette VB, Seja E, Vu HT, et al. Role of dendritic cell phenotype, determinant spreading, and negative costimulatory blockade in dendritic cell-based melanoma immunotherapy. J Immunother 2004;27:354–67.
34. Tumeh PC, Harview CL, Yearley JH, Shintaku IP, Taylor EJ, Robert L, et al. PD-1 blockade induces responses by inhibiting adaptive immune resistance. Nature 2014;515:568–71.
35. Kim D, Pertea G, Trapnell C, Pimentel H, Kelley R, Salzberg SL. TopHat2: accurate alignment of transcriptomes in the presence of insertions, deletions and gene fusions. Genome Biol 2013;14:R36.
36. Trapnell C, Williams BA, Pertea G, Mortazavi A, Kwan G, van Baren MJ, et al. Transcript assembly and quantification by RNA-Seq reveals unannotated transcripts and isoform switching during cell differentiation. Nat Biotechnol 2010;28:511–5.

Chapter 2

Melanoma dedifferentiation induced by interferon-gamma epigenetic remodeling in response to anti-PD-1 therapy

Introduction

Cancer immunotherapy has remarkably improved the treatment landscape for advanced melanoma, a highly aggressive skin cancer with traditionally dismal survival outcomes. Melanoma is the result of a malignant transformation of melanocytes, which develop from neural crest cells during embryogenesis (Restivo et al., 2017; Yoshida et al., 1996). The melanoma cancer cells arise from different stages of differentiation between the neural crest precursors and fully differentiated melanocytes (Hoek et al., 2008; Restivo et al., 2017; Tirosh et al., 2016; Tsoi et al., 2018). Not only are melanomas highly heterogeneous, they also display a large degree of plasticity that is highlighted by the ability of the differentiated cancer cells to dedifferentiate to a more neural crest phenotype.

Melanoma dedifferentiation is defined by the loss of melanosomal antigens such as the melanoma antigen recognized by T cells 1 (MART-1/ Melan-A) or gp100, with the concomitant gain of neural crest markers such as the nerve growth factor receptor (NGFR or CD271) or AXL (Müller et al., 2014; Nazarian et al., 2010; Tirosh et al., 2016). The expression of the melanosomal antigens is driven by the melanocyte inducing transcription factor (MITF), the master regulator of melanoma differentiation (Opdecamp et al., 1997; Tachibana et al., 1996). Therefore, the downregulation of MITF is a major feature of dedifferentiation. This phenotypic plasticity has been associated with therapeutic resistance to BRAF inhibitors and with drug-resistant persister cells (Konieczkowski et al., 2014; Müller et al., 2014; Rambow et al., 2018; Tirosh et al., 2016; Tsoi et al., 2018). It has also been shown to be a resistance mechanism against MART1

antigen-specific T cell adoptive cell transfer therapy in both mice and humans. Furthermore, the pro-inflammatory cytokine tumor necrosis factor (TNF) was shown to induce this dedifferentiation (Landsberg et al., 2012; Mehta, Kim et al., 2018). The TNF-induced dedifferentiation was reversible with the removal of immune stimulation (Mehta, Kim et al., 2018), suggesting that transcriptomic mechanisms may be at play.

Despite the multitude of studies on melanoma plasticity, its role in the context of immune checkpoint blockade therapy has not been elucidated. In fact, direct and indirect evidence has led to the postulation that dedifferentiation would be a state of resistance to immunotherapy for melanoma (Falletta et al., 2017; Hölzel & Tüting, 2016). Therefore, we investigated whether dedifferentiation results in therapeutic resistance to PD-1 blockade therapy in patients with advanced melanoma.

Results

Loss of melanocytic lineage markers is associated with clinical response to immune checkpoint blockade

To study the effect of melanocyte lineage differentiation state, we analyzed paired and unpaired baseline and on-therapy biopsies of patients receiving immune checkpoint blockade (ICB) therapy from the CheckMate 038 clinical trial. This was a prospective, multicenter, international, multi-cohort clinical trial designed to collect tumor biopsies from patients with metastatic melanoma treated with the anti-PD-1 antibody nivolumab as front-line therapy or after progressing on therapy with the anti-cytotoxic T cell antigen 4 (CTLA-4) antibody ipilimumab, or receiving the combination of both antibodies (Riaz et al., 2017; Grasso et al., under review). Of the 101 patients, 68 had paired biopsies, and of those paired, 27 were from patients with progressive disease (PD), 14 with stable disease (SD), and 27 with complete response or partial response (CRPR). On-therapy biopsies, collected at approximately one month after starting on ICB therapy, had notable downregulation of *MITF* and *MLANA* and concomitant upregulation of *AXL* only from the CRPR group. The biopsies from the SD and PD groups did not display significant changes in *MITF*, *MLANA*, or *AXL* following treatment (Figure 1A). This observation is at odds with the conventional view of dedifferentiation as a resistance mechanism and indicates that dedifferentiation may serve as a marker of favorable response to immune checkpoint blockade. As the presence of interferon-gamma (IFNγ) signatures in biopsies is best correlated with response to the anti-PD-1 therapy (Ayers et al., 2017; Cristescu et al.,

2018; Grasso et al., under review), we hypothesized that the dedifferentiation of these responding tumors may be mediated by continued exposure to T cells producing IFNγ.

In vitro modeling of cytokine-induced melanoma dedifferentiation

Previously, it has been reported that human melanoma cell lines can be categorized into four subtypes based on their differentiation states: Melanocytic, transitory, neural crest-like, and undifferentiated (Tsoi et al., 2018). The cell lines that are baseline melanocyte differentiated, characterized by high expression of MART1 and no expression of neural crest marker NGFR, have an ability to become dedifferentiated upon exposure to TNF or a BRAF inhibitor (Landsberg et al., 2012; Tsoi et al., 2018).

To test whether IFNγ induces this same phenotypic change, we established an *in vitro* system to model the phenotypic plasticity. Four baseline differentiated human melanoma cell lines (M262, M308, M399 and 3998mel) were treated continuously with human recombinant IFNγ and the change in phenotype was compared to the dedifferentiation induced by three days of TNF, which served as a positive control for melanoma dedifferentiation. Flow cytometry using fluorescent anti-MART1 and anti-NGFR antibodies revealed dedifferentiation of these four cell lines over the course of two to five weeks (Figure 1B & S1A). The duration of continuous IFNγ exposure needed to reach the maximal MART1-low, NGFR-high state varied for each cell line but were comparable to the approximate one-month time point at which the aforementioned biopsies were taken during the course of the anti-PD-1 therapy in patients. In addition, in four human melanoma cell lines that were baseline undifferentiated (M257A2, M370, M381 and

M410), neither cytokines induced dedifferentiation. Interestingly, continuous IFNγ exposure led to what appears to be redifferentiation of some of these cell lines. The cells increased NGFR levels with no change in MART1 levels, a reversal of the last step of the previously described melanoma dedifferentiation trajectory from neural crest-like to undifferentiated (Tsoi et al., 2018) (Figure 1B & Fig S1A).

Concordant transcriptomic programs reflect the phenotypic plasticity driven by IFNγ and TNF

To study the mechanism of this cytokine-induced cellular plasticity, we performed whole transcriptome RNA sequencing (RNA-seq) and assay for transposase-accessible chromatin sequencing (ATAC-seq) on the aforementioned eight cell lines, four that were differentiated at baseline and dedifferentiate with IFNγ exposure, and four that were undifferentiated at baseline and did not differentiate further with continuous IFNγ exposure, as well as the same cell lines exposed to three days of TNF as positive control (Figure 1B).

To assess the effect of cytokine treatment on the melanoma transcriptome, we projected all samples onto a previously defined principal component analysis (PCA) framework of 54 baseline human melanoma cell lines spanning the four defined differentiation states (Tsoi et al., 2018). As expected, the projection of the eight cell lines segregated according to the baseline differentiation status, with the dedifferentiated samples from either cytokine shifting towards a more neural crest-like state within the defined dedifferentiation trajectory (Figure 1C). We also interrogated the gene expression profiles of our samples

for the enrichment of previously defined gene signatures for various melanoma differentiation states, from melanocytic (M) to undifferentiated (U). Clear downregulation of the melanocytic subtype signature was observed with either cytokine-driven dedifferentiation, with the concomitant enrichment of the neural crest or transitory subtype signatures (Figure 1D). There were no distinguishing patterns between the two groups of cell lines in terms of nonsense or missense mutations in well-studied, relevant genes that may contribute to the observed differences (Figure 1E). In addition, neither group harbored consequential mutations in genes that code for critical members of the IFNγ response pathway, as previously reported in melanoma tumors (Shin et al., 2017; Zaretsky et al., 2016), suggesting that these lines all activate IFNγ-dependent transcription factors upon stimulation (Figure S1B, S2A-B).

In order to identify commonly induced genes across all cell lines, we performed partial least squares regression (PLSR) on baseline versus cytokine-exposed cell lines. All eight samples had clear cytokine responses regardless of their baseline differentiation status (Figure 2A and 2C), which ensures that the difference in phenotype is not attributable to any lack of cytokine response in one group. Ranking of the genes induced by continued IFNγ exposure across the eight cell lines revealed upregulation of *IRF1*, *SOSC1* and *STAT1* (Figure 2B). The K-means clustering of the top 300 upregulated genes revealed a cluster of genes that were commonly induced to similar levels in both baseline-differentiated and undifferentiated lines upon continued IFNγ exposure (Figure 2B). It also revealed a distinct cluster of genes that were strongly induced in only the undifferentiated lines (Figure 2B), which suggests induction of a transcriptional response from these cell

lines despite their already dedifferentiated state. The clusters of genes highly upregulated in the dedifferentiating group were also upregulated to similar levels in the baseline undifferentiated group, which indicates that the IFNγ downstream signaling is preserved regardless of the differentiation status and suggests that epigenetic differences not captured by the gene expression analysis may be responsible for the diverging plasticity. The ranking of genes induced by TNF across the eight cell lines pointed at much stronger upregulation of *TNF*, *TNFAIP3*, and *NFKBIA* in comparison to their rank in the IFNγ analysis (Figure 2D). The K-means clustering of the top 300 upregulated genes revealed a cluster of genes that were much more strongly induced in the samples that dedifferentiate, indicating a transcriptional program induced by TNF that is unique to cells capable of the phenotypic switch. We additionally looked at the cross enrichment of one cytokine with the top 300 induced genes from the other. The TNF matrix with the top 300 IFNγ -induced genes and the IFNγ matrix with the top 300 TNF-induced genes showed similar levels of induction (Figure S2C-D).

To determine whether the IFNγ- and TNF-induced dedifferentiation states had similar gene expression profile changes, we performed rank-rank hypergeometric overlap (Plaisier, Taschereau, Wong, & Graeber, 2010). Significant overlap in IFNγ- and TNF-induced genes were revealed (Figure 2E), with an even higher degree of overlap at the level of gene sets (Figure 2F). This data indicates concordant gene programs despite the difference in inducible expression of individual genes. Examining the enrichment of the terms from GSEA, or GSEA-squared (Balanis et al., 2019), confirmed the loss of

pigmentation with the gain of inflammatory signaling following IFNγ and TNF exposures (Figure 2G and 2H).

TNF and IFNγ induce dedifferentiation via distinct global chromatin landscape alterations

Evaluation of the ATAC-seq tracks at the promoter of *MLANA* revealed no basal chromatin accessibility in undifferentiated cell lines along with a decrease of chromatin accessibility of differentiated cell lines upon IFNγ - or TNF-induced dedifferentiation, consistent with the flow cytometry and RNA-seq data (Figure 3A). ATAC-seq tracks at the promoter of *AXL* also reveal the pattern expected, with no changes in the baseline undifferentiated lines upon cytokine exposure and increased peaks in the baseline differentiated lines when they dedifferentiate upon cytokine exposure (Figure 3A). Pair-wise comparisons of cytokine-stimulated to unstimulated cell lines revealed between 2500 and 7000 peaks that were hyperaccessible following either IFNγ or TNF exposure (Figure 3B). Interestingly, IFNγ induced a similar number of hyperaccessible peaks for both the baseline differentiated and the undifferentiated lines, but TNF induced a large number of hyperaccessible peaks only in baseline differentiated lines (Figure 3B). Principal component analysis of all induced ATAC-seq peaks showed that the baseline differentiated and the undifferentiated cell lines exist in two different epigenomic states. TNF exposure in undifferentiated cell lines caused minimal epigenetic changes but drove drastic changes toward the undifferentiated state in the baseline differentiated ones, consistent with the transcriptional response (Figure 3C). The baseline differentiation states and the shared phenotypic change due to IFNγ and TNF were best represented

by PC1, whereas PC2 best defined the divergence in the effects of the two cytokines, revealing the IFNγ-specific response. Despite inducing the comparable changes in NGFR and MART1 status based on protein expression, the exposure to either of the two cytokines resulted in distinctive chromatin alterations which manifest as a shift along one or both axes of the PCA analysis. Of note, PC2 also supported the redifferentiation phenomenon (Figure 3C) observed in the flow cytometry data (Figure 1B, S1A).

K-means clustering of accessible chromatin peaks induced by either cytokine revealed patterns that corroborated the PCA observations. The first cluster revealed that chromatin regions that were largely closed initially and only weakly induced in the dedifferentiating cell lines following cytokine stimulation were accessible in the undifferentiated cell lines at baseline and remained so after TNF exposure. This suggests the presence of a high baseline signaling pathway that may be responsible for the lack of further response to stimulation by TNF. The second cluster revealed that IFNγ induced opening of chromatin regions more uniformly across the cell lines regardless of their baseline differentiation status, which was reflected in the large magnitude of change observed in the above PCA in all eight of the cell lines following IFNγ. Lastly, the third cluster revealed a group of peaks that were strongly induced by TNF, in the dedifferentiating cell lines only (Figure 3D).

K-means clustering of the induced ATAC peaks at the transcriptional start sites similarly indicated that undifferentiated cell lines had a more open chromatin at baseline (Figure S3A). Motif enrichment analysis of the ATAC peaks revealed distinct clusters of

transcription factors whose binding sites were opened upon IFNγ or TNF exposure. Notably, no common motifs were enriched to comparable levels in the IFNγ- and TNF-induced peaks. The motifs of select IRF proteins were the most highly enriched following IFNγ, while the motifs of the ATF3, BATF, and AP-1 family factors were the most highly enriched following TNF, even more so than those of NFκB (Figure 3E, S3B). Both TNF and IFNγ exposure led to largely hyperaccesible chromatin in intergenic regions that were associated with axon guidance and cell migration (Figure 3F). However, their effects were distinct in that TNF opened chromatin regions near genes associated with mitogen-activated protein kinase (MAPK) pathway, neuronal system, and growth factor signaling, while IFNγ generated stronger enrichment for chromatin regions near genes involved in interferon response and antigen presentation (Figure 3F).

Motif enrichment analysis of hyperaccessible chromatin regions following IFNγ and TNF exposure reveal regulators involved in dedifferentiation

We next asked how the baseline differentiation states of the melanoma cell lines, their baseline epigenomic profiles and signaling network, affected their response to IFNγ stimulation. Although similar numbers of peaks were found to be inducible by IFNγ in baseline differentiated and undifferentiated cell lines, there was minimal overlap in the induced regions, and neither of the inducible peaks overlapped significantly with TNF inducible peaks (Figure 4A-B). Thus, although both TNF and IFNγ lead to a parallel transition to the dedifferentiated phenotype defined by similar gene programs, their effects on the chromatin landscape were stimulus-specific. Notably, the undifferentiated cell lines had minimal chromatin remodeling in response to response to TNF, despite the observed

changes in gene expression. In addition, when exposed to continuous IFNγ, these lines had comparable level of remodeling to that of the baseline differentiated cell lines although they do not undergo further phenotypic dedifferentiation. As the majority of the two groups' IFNγ-induced peaks did not overlap (Figure 4B), the overall response to IFNγ seems to depend on the cell line's baseline epigenomic state.

In order to dissect out peaks that may be attributable to the differences in phenotypic plasticity, all the peaks that were significantly induced from baseline by either IFNγ or TNF were used to perform K-means clustering. While clusters of peaks that were partial to either baseline differentiated or undifferentiated cell lines were revealed, cell line heterogeneity was also evident (Figure 4C). Interestingly, the top transcription factors whose motifs were enriched in the induced peak regions were common across all three clusters for both cytokines. This suggests that, of all IRF1 or IRF2 binding sites throughout the genome that open in response to IFNγ, certain sites selectively open in undifferentiated cell lines (Figure 4C). Similarly, of all ATF3 or BATF binding sites in the genome, certain sites open only in the cell lines that dedifferentiate in response to TNF (Figure 4C).

Upon IFNγ exposure, most IRF and STAT binding sites become hyperaccessible in baseline differentiated and undifferentiated groups except for STAT6. The binding motifs of STAT6 and AP-2 proteins were enriched in the peaks in dedifferentiating cells only, driven by either cytokine. Despite solely having exposure to type II interferon and no expression of IFNA or IFNB, the IFNγ-exposed samples showed chromatin remodeling

fitting for exposure to type I interferon. This finding supports that there is direct secondary activation of such factors as a result of exposure to IFNγ. Notably, there was enrichment for binding sites of IRFs whose activities were known to be restricted to other cell types, such as IRF8 in dendritic cells. Upon TNF exposure, the inducible peaks were highly enriched in IRFs and STATs binding sites only in the dedifferentiating group, indicating that the phenotypic plasticity is driven by the crosstalk with the IFN pathway or by secondary activation of the regulators downstream of the IFN pathway (Figure 4D).

TNF is known to trigger the MAPK pathways, which lead to transcription factor activity of ATF and AP-1 proteins. Motif enrichment analysis revealed that the TNF stimulus lead to the opening of the binding sites of AP-1 factors (Fosl1, Jun-AP, JunB, AP-1, c-Jun, JunD) following TNF-induced dedifferentiation, with no enrichment of these motifs in the inducible peaks of the undifferentiated cell lines following TNF exposure. On the contrary, the inducible peaks from all samples treated with IFNγ, regardless of baseline differentiation state, exhibited enrichment of the AP-1 family protein motifs (Figure 4D). In addition, PRDM1 was another factor whose motif had enrichment only in TNF-induced peaks, while the motif for Oct4:Sox17 was only enriched in IFNγ-induced peaks. Altogether, these data show that the baseline epigenomic state of the melanoma cells is the determinant of the resultant differential chromatin landscape modifications from IFNγ or TNF cytokine exposure.

Inferred regulator activity analysis suggests common regulator activity changes between TNF- and IFNγ-induced dedifferentiation

Given the similar binding motifs within families of transcription factors, such as within several IRFs, the NFκB family proteins, and MAPK-activated transcription factors, we next explored the inferred activity of these candidate immune-signaling transcription factors. Using ARACNe (Algorithm for the Reconstruction of Accurate Cellular Network), which uses mutual information to connect regulators and target genes, we constructed reverse-engineer melanoma-specific, IFNγ-response-specific transcriptional networks. We next employed VIPER (Virtual Inference of Protein Activity by Enriched Regulon) to infer the differential activity of over 9000 regulators in cytokine treated versus baseline cell lines. In both TNF- and IFNγ-exposed cell lines, the regulators TFAP2C (AP-2gamma), SOX9, IRF3, and HMGA1 had high inferred activity only with dedifferentiation, confirming the ATAC-seq data. On the other hand, MITF, beta-catenin, and SOX10 had decreased inferred activity only in the dedifferentiating cell lines. In addition, transcription factors PRDM1, NFKBIA, RXRB, and POU2F2 had positive change in activity in both groups, albeit having higher activity in the dedifferentiating group (Figure 5A and 5B). In addition, the comparison of this gene expression level-derived inferred activity of regulators between TNF and IFNγ-exposed samples showed strong overlap of inferred activity changes in response to each cytokine (Figure S4A-D).

Changes in lipid, ribosomal, mitochondrial, and adhesion processes distinguish the TNF- or IFNγ-induced responses in baseline differentiated versus undifferentiated cell lines

To increase our understanding of this new effect of IFNγ on melanoma cells, we performed analysis of the molecular and cellular changes defining pro-inflammatory

cytokine-driven dedifferentiation. We used GSEA-squared analysis on gene expression signatures for differentiated and undifferentiated cell line groups exposed to IFNγ or TNF, and looked for the enrichment of programs and processes of interest. As expected, immune-related terms were highly enriched in all groups. Both differentiated and undifferentiated TNF-treated cell lines displayed enrichment of NFκB and immune response genes. However, while differentiated lines displayed strong downregulation of ribosomal and mitochondrial genes and upregulation of adhesion-related genes, undifferentiated cell lines did not, or in the case of mitochondrial genes, not to the extent observed in the differentiated cell lines. In contrast, undifferentiated lines showed stronger upregulation of lipid gene sets. Thus, as all lines upregulate immune and inflammatory programs, but the undifferentiated cell lines do not change phenotype with TNF, the differences in TNF-induced chromatin remodeling observed between differentiated and undifferentiated lines is correlated with control of lipid, ribosomal, mitochondrial and adhesion gene programs (Figure 6A).

For IFNγ, in the both the differentiated and undifferentiated samples, immune response gene programs are commonly upregulated, while ribosomal and mitochondrial gene sets were downregulated. Consistent with differentiated and undifferentiated lines exhibiting more equal magnitude of IFNγ-induced chromatin accessibility changes, there were also fewer divergent gene set categories between these two groups under IFNγ exposure. (Figure 6B).

Enrichment of the IFNγ-induced dedifferentiation signature during anti-PD-1 therapy is associated with response

Dedifferentiation of melanoma has been considered a form of resistance to therapy and associated with worse survival of patients (Konieczkowski et al., 2014; Müller et al., 2014; Tirosh et al., 2016; Rambow et al., 2018; Tsoi et al., 2018). However, because we observed the opposite correlation between high AXL to MITF ratio in biopsies of patients who were responding to anti-PD-1 therapy, we sought to further investigate whether the full IFNγ-driven dedifferentiation signature correlated with therapeutic response. From the seven signatures (four main signatures, three transitional signatures) spanning the four previously defined melanoma subtypes obtained from a previous study (Tsoi et al., 2018), the melanocytic subtype was excluded, and the remaining genes were filtered for the genes with log2(fold change) of greater than 1 with IFNγ treatment. These select upregulated genes henceforth comprised our IFNγ-induced dedifferentiation signature and was used to interrogate the CheckMate 038 biopsy cohort. Increase in the expression of the signature was found following anti-PD-1 therapy in the patients with objective response (CRPR), with no significant changes from baseline in non-responders (Figure 7A). Therefore, biopsies of patients taken while responding to PD-1 blockade therapy show phenotypic dedifferentiation, while non-responding biopsies did not change their differentiation state.

Baseline dedifferentiation in melanoma associates with response to anti-PD-1 therapy and improves outcomes

Finally, we analyzed if the IFNγ-induced dedifferentiation signature could be a baseline prognostic or predictive marker in the CheckMate 038 biopsy cohort and in the melanoma The Cancer Genome Atlas (TCGA) repository. There was a significant spread in the expression of the IFNγ-induced dedifferentiation signature at baseline in the CheckMate 038 biopsy cohort, but separation of these 101 baseline biopsies according to response to therapy showed that the biopsies of patients who went onto respond were more likely to have an increased IFNγ-induced dedifferentiation signature ($p = 0.06$ by Wilcoxon test, Figure 7B). Moreover, the IFNγ-induced dedifferentiation signature also correlated positively with overall survival in the TCGA melanoma dataset. Patients whose melanomas had high or intermediate expression of the IFNγ dedifferentiation signature displaying improved overall survival than those with low expression of the signature (Figure 7C).

Discussion

Here we report a previously unobserved facet of IFNγ, whereby continuous exposure to IFNγ propels melanoma cells toward an altered phenotype with diminished expression of melanosomal markers and increased expression of neural crest markers. Moreover, we demonstrate that melanoma cells exposed to IFNγ and TNF reach two distinct epigenomic states of dedifferentiation despite displaying similar phenotypic dedifferentiation. IFNγ elicited pronounced remodeling of the chromatin landscape in all tested melanoma cell lines regardless of the baseline differentiation status.

We observed in our data a number of regulators that have been implicated in melanocyte differentiation, and it is possible that the change in the activity of these regulators may facilitate the backward trajectory. For one, beta-catenin activity was inferred to be decreased in response to TNF- and IFNγ-induced dedifferentiation based on our VIPER analysis, and Wnt/beta-catenin signaling is known to play a role in human melanocyte development from neural crest cells (Bellei, Pitisci, Catricalà, Larue, & Picardo, 2011). AP-1 has been linked to dedifferentiation in the setting of TNF-induced dedifferentiation in mouse models (Riesenberg et al., 2015), and we observed that it was one of the top enriched motifs in the chromatin regions opened in TNF-dedifferentiated cells and also in IFNγ-dedifferentiated cells, albeit to a much lesser degree. On the other hand, our analyses also reveal transcription factors with previously unknown involvement in the phenotypic plasticity of human melanomas.

Contrary to the conventional belief that dedifferentiation is a state of therapeutic resistance (Konieczkowski et al., 2014; Müller et al., 2014; Tirosh et al., 2016; Rambow et al., 2018; Tsoi et al., 2018), we show that the consequence of this phenotypic plasticity depends on the context of the therapy. While it is a resistance mechanism against adoptive cell transfer using T cells against a specific melanosomal antigen (Landsberg et al., 2012; Mehta, Kim et al., 2018), we show that it is a surrogate marker for positive response to immune checkpoint blockade therapy. Tumor infiltration by tumor-specific T cells results in triggering their T cell receptor (TCR) and downstream IFNγ production upon antigen encounter, which is the mechanistic basis of responses to anti-PD-1 therapy and favorable prognostic factors. One of the advantages of IFNγ signaling in cancer cells is the reactive expression of the PD-1 ligand 1 (PD-L1), which provides a mean for the cancer cells to protect themselves from tumor antigen-specific T cell killing (Ribas & Wolchok, 2018). These T cells continue to be present in specific regions of the tumor (Tumeh et al., 2014), and their production of IFNγ is a favorable prognostic factor that can be detected by a transcriptome of IFNγ response genes (Ayers et al., 2017; Cristescu et al., 2018; Grasso et al., under review). Once the negative interaction between PD-1 and PD-L1 is released by checkpoint therapies, the antitumor T cells proliferate and produce increased IFNγ leading to an amplification of the antitumor immune response that mediates the clinical benefits (Ribas & Wolchok, 2018; Tumeh et al., 2014; Grasso et al., under review). Therefore, our observation that responding melanoma biopsies undergo dedifferentiation is highly concordant with our discovery that continuous exposure to IFNγ in differentiated melanomas leads to this phenotypic change.

Moreover, both in the anti-PD-1 treated cohort and in the TCGA melanoma database we noted that the IFNγ-induced dedifferentiation transcriptional signature was associated with improved outcomes. In both cases, it is likely that the dedifferentiation is an indirect reflection of IFNγ produced by tumor antigen-specific T cells. However, as only melanomas that are originally phenotypically differentiated can undergo dedifferentiation upon chronic IFNγ exposure, in these two series the baseline dedifferentiation group is likely to include both melanomas that were originally dedifferentiated independent of a T cell response, and originally differentiated melanomas that dedifferentiate upon T cell recognition and IFNγ production. This dual mechanism leading to dedifferentiation results in difficulty in interpreting the patient biopsy data.

It has been shown that IFNγ from skin-infiltrating CD8+ cytotoxic T cells can inhibit expression of MITF in normal melanocytes (Yang et al., 2015), indicating that this phenotypic response to pro-inflammatory cytokines may be conserved from melanocytes to melanomas. Therefore, the ability to change the phenotype upon cytokine exposure may have biological advantages that are independent of the malignant transformation of melanocytes. The specific mechanism of how IFNγ leads to the loss of MITF and gain of neural crest lineage markers is unknown; nonetheless, this study helps to elucidate the epigenetic landscape that characterizes the new phenotypic endpoint driven by IFNγ and the transcriptional regulators that may be partaking in eliciting this change. In summary, melanoma dedifferentiation can be induced by chronic IFNγ exposure and is associated with improved outcomes in patients with melanoma.

Acknowledgements

We would like to thank Stephen T. Smale at UCLA for kindly sharing his expertise and providing guidance. We would like to thank Hong Zhang at the Technology Center for Genomics and Bioinformatics Core Facility at UCLA for her helpful discussions on ATAC-sequencing. We would also like to thank Alena Gros for kindly sharing the cell line 3998mel. Y.J.K. was supported by the NIH Ruth L. Kirschstein Institutional National Research Service Award F30 CA243248 and the NIH NIGMS training grant T32-GM008042. K.M.S. was supported by the NIH NIGMS training grant T32-GM008042 and T32-GM008185. J.T. was supported by the NIH T32-CA009120. G.A-R. was supported by the Isabel & Harvey Kibel Fellowship award and the Alan Ghitis Fellowship Award for Melanoma Research. D.Y.T. was supported by a Young Investigator Award from ASCO, a grant from the Spanish Society of Medical Oncology for Translational Research in Reference Centers and the V Foundation-Gil Nickel Family Endowed Fellowship in Melanoma Research. A.H. was funded by NIH grant R01AI132835. C.P.S. is a recipient of a Parker Senior Fellow Award from the Parker Institute for Cancer Immunotherapy. T.G.G. and A.R. were funded by NIH grant P01 CA168585. A.R. was funded by the Parker Institute for Cancer Immunotherapy, NIH grants R35 CA197633, and P30 CA016042, the Ressler Family Fund, Ken and Donna Schultz Fund, and Cancer Immunology Translational Cancer Research Grant (SU2C-AACR-DT1012) from Cancer Research Institute–Stand Up 2 Cancer. Stand Up 2 Cancer is a program of the Entertainment Industry Foundation administered by the American Association for Cancer Research.

Author Contributions

A.R. conceived and supervised the project. Y.J.K. and A.R. designed the experiments and interpreted the results. Y.J.K conducted the research and analyzed the data. K.M.S. and Y.J.K. decided on the bioinformatic approaches and analyses. K.M.S. performed the ATAC-seq and RNA-seq bioinformatic analyses. J.T. performed RNA-seq processing and bioinformatic analyses. J.T., G.A-R., E.M., and C.S.G. performed analysis of the clinical biopsy cohort. D.Y.T., A.S.C., K.L., C.S., D.E.S., P.O.S., A.H., T.G.G., and C.P-S. contributed technical and scientific expertise for experimental design or analysis. Y.J.K., K.M.S., and A.R. wrote the manuscript with input from the co-authors. All authors reviewed and approved the manuscript.

Declaration of Interests

K.L. reports speaker fees from Roche Tissue Diagnostics. C.S. reports grant support from Pfizer, AstraZeneca, BMS, Roche-Ventana, Boehringer-Ingelheim, and Ono. C.S. has consulted for Pfizer, Novartis, GlaxoSmithKline, MSD, BMS, Celgene, AstraZeneca, Illumina, Genentech, Roche-Ventana, GRAIL, Medicxi, and the Sarah Cannon Research Institute. C.S. is a shareholder of Apogen Biotechnologies, Epic Bioscience, GRAIL, and has stock options in and is co-founder of Achilles Therapeutics. T.G.G. reports receiving an honorarium from Amgen, and having consulting and equity agreements with Trethera Corporation. The lab of T.G.G. has completed a research agreement with ImmunoActiva. A.R. has received honoraria from consulting with Amgen, Bristol-Myers Squibb, Chugai, Genentech, Merck, Novartis, Roche and Sanofi, is or has been a member of the scientific advisory board and holds stock in Advaxis, Apricity, Arcus Biosciences, Bioncotech Therapeutics, Compugen, CytomX, Five Prime, FLX-Bio, ImaginAb, Isoplexis, Kite-Gilead, Lutris Pharma, Merus, PACT Pharma, Rgenix and Tango Therapeutics, has received research funding from Agilent and from Bristol-Myers Squibb through Stand Up to Cancer (SU2C).

Figure Titles and Legends

Figure 1. Human melanoma dedifferentiation is associated with response to anti PD-1 therapy and is induced by exposure to IFNγ. A) *MITF, MLANA, and AXL* gene expression levels in pre- and post-treatment biopsies from patients with progressive disease (PD), stable disease (SD), and complete or partial response (CRPR). B) Flow cytometry data for MART1 and NGFR on M262 (baseline differentiated) and M370 (baseline undifferentiated) in response to TNF or IFNγ. C) Projection of cytokine-treated cell lines onto melanoma M series differentiation PCA (Tsoi et al.). Diff = baseline differentiated, undiff = baseline undifferentiated. D) Expression of melanoma differentiation genes for 0hr, IFNγ, and TNF across cell lines (U= Undifferentiated, U-NC= Undifferentiated-Neural crest-like, NC= Neural crest-like, NC-T= Neural crest-like-Transitory, T= Transitory, T-M= Transitory-Melanocytic, M= Melanocytic). Colors represent z scores. E) Common melanoma mutations across cell lines studies. Nonsense or missense JAK/STAT mutations were not observed.

Figure 2. IFNγ and TNF stimulation induce common genes across cell lines to generate comparable MART1-low/NGFR-high dedifferentiation states. A) Varimax-rotated PLSR on IFNγ-exposed compared to 0 hour (untreated) samples. B) (left) Genes contributing to common IFNγ response across samples. (right) K-means clustering of top 300 gene loadings. Left column is untreated and right column is post-IFNγ exposure for each cell line. C) Varimax-rotated PLSR on TNF compared to untreated samples. D) (left) Genes contributing to TNF response across samples. (right) K-means clustering of top 300 gene

loadings. Left column is untreated and right column is post-TNF exposure for each cell line. E) Overlap of IFNγ and TNF induced gene expression by ranked loadings. F) Concordant gene ontology term overlap (normalized enrichment scores) between IFNγ and TNF-induced gene expression. G-H) Enrichment of gene sets involving pigmentation, mitosis, transcription, interferon signaling, and cytokines following IFNγ or TNF exposure.

Figure 3. IFNγ compared to TNF alter the chromatin landscape in a stimulus-specific manner. A) Examples of hyperaccessible peaks upon cytokine stimulation. B) Total number of hyper and hypoaccessbile peaks called for each listed comparison (U = Undifferentiated at baseline, D = Differentiated at baseline). C) PCA of peaks differentially hyperaccessible from baseline after cytokine treatment. D) K-means clustered heatmap of induced ATACseq peaks across any stimulation condition for differentiated and undifferentiated melanomas (sub-columns are in the order 0 hr, IFNγ, and TNF for each cell line). E) Motif enrichment of IFNγ compared to TNF induced genes. F) Top divergent gene ontology terms of nearby genes for IFNγ compared to TNF-specific peaks.

Figure 4. The basal chromatin landscapes of differentiated and undifferentiated lines result in distinct epigenomic responses upon cytokine stimulation. A) Overlap of induced IFNγ and TNF ATACseq peaks. B) Overlap of peaks separated by cell line baseline state (Diff = baseline differentiated, Undiff = baseline undifferentiated). C) Heatmap of differentially IFNγ inducible peaks for baseline differentiated and undifferentiated lines, with top motif of each cluster listed (sub-columns are in the order 0 hour, IFNγ, and TNF for each cell line). D) Heatmap of differentially TNF inducible peaks for baseline

differentiated and undifferentiated lines, with top motif of each cluster listed. D) Motif enrichment of IFNγ compared to TNF inducible peaks for baseline differentiated and undifferentiated lines separately (U= baseline undifferentiated, D = baseline differentiated). Colors represent q values.

Figure 5. Differentiated and undifferentiated lines respond to cytokine stimulation with differences in inferred activity of both signal-dependent and lineage determining transcription factors. A-B) VIPER analysis showing inferred TF activity for baseline differentiated versus undifferentiated lines following (A) TNF or (B) IFNγ exposure. Regulators such as PRDM1, HMGA1, SOX9 have high inferred activity only in the baseline differentiated group.

Figure 6. Gene expression differences between differentiated and undifferentiated lines may be attributed to lipid, ribosomal, mitochondrial, and adhesion processes. A-B) Enrichment of gene set groups (C5: GO gene sets) based on ranked lists of differentially expressed genes, for TNF or IFNγ.

Figure 7. The enrichment of IFNγ-induced dedifferentiation gene signatures in melanomas correlate with response to anti-PD-1 and better overall survival. A) Enrichment of the dedifferentiation signature in the paired pre- and post-treatment biopsies (n=68) of responders and non-responders from the Checkmate 038 biopsy cohort. B) Enrichment of the dedifferentiation signature in the baseline biopsies of the Checkmate 038 biopsy cohort, including the paired and unpaired biopsies (n=101), from

responders and non-responders. C) Correlation of baseline enrichment of the dedifferentiation signature with overall survival in the TCGA melanoma dataset.

Supplemental Figure Legends

Figure S1. Related to Figure 1. IFNγ and TNF drive loss of MART1 and gain of NGFR expression in baseline differentiated cell lines and baseline differentiation status of cell lines is not governed by their mutation status. A) Flow cytometry plots of baseline differentiated cell lines (left) and baseline undifferentiated cell lines (right) upon IFNγ or TNF exposure. B) Mutation status of the eight cell lines for select relevant genes.

Figure S2. Related to Figure 2. A) PCA of gene expression on all genes. B) Signature score of each sample based on genes in "GO_Interferon-gamma mediated signaling pathway" shows all samples upregulated IFNγ-related response genes. C) TNF samples (left) for IFNγ signature genes. D) IFNγ samples (right) for TNF signature genes.

Figure S3. Related to Figure 3. A) K-means clustering of the induced ATAC-seq peaks, with their positions relative to the transcriptional start sites. B) Top enriched motifs in the hyperaccesible ATAC peaks of TNF- and IFNγ-exposed cell lines.

Figure S4. **Related to Figure 5.** A-B) VIPER analysis plots showing inferred TF activity for differentiated versus undifferentiated lines for (A) TNF or (B) IFNγ. C-D) TNF and IFNγ comparisons of each baseline differentiation status.

Methods

Patient Biopsy Samples and RNA-Sequencing

Study CheckMate 038 (NCT01621490) was a multi-arm, multi-institutional, prospective study to investigate the effects of nivolumab (3 mg/kg every 2 weeks) single agent, or the combination of nivolumab (1 mg/kg every 3 weeks) plus ipilimumab (3 mg/kg every 3 weeks) given for four doses and followed by nivolumab (3 mg/kg every 2 weeks) single agent. The protocol and its amendments were approved by the relevant institutional review boards, and the study was conducted in accordance with the Declaration of Helsinki and the International Conference on Harmonization Guidelines for Good Clinical Practice. All patients signed written informed consent prior to having any study procedures performed. Patients were treated until progression or for a maximum of 2 years, or were stopped due to toxicities. Radiographic assessment of response was performed approximately every 8 weeks until progression. Progression was confirmed with a repeat CT scan at least four weeks later. Tumor response for patients was defined by RECIST v1.1. Response to therapy indicates best overall response unless otherwise indicated. All patients underwent a baseline biopsy before commencing therapy (1 to 7 days before the first dose of therapy) and a repeat biopsy, on cycle 1, day 29 (between days 23–29).

Baseline and on-therapy tumor tissue biopsies were stored with RNAlater (Ambion) for subsequent RNA extraction using Qiagen kits. Of 170 patients, 101 had enough RNA for RNAseq (Figure 1). RNA-seq library was prepared using Illumina Truseq Stranded mRNA kit. Sequencing was done on an Illumina HiSeq sequencer using paired end

sequencing of 50 bp for each mate pair. RNA-seq reads were mapped using HISAT2 version 2.0.4 (Kim, Paggi, Park, Bennett, & Salzberg, 2019) and aligned to the hg19 genome using default parameters. Reads were quantified by HTSeq version 0.6.1 (Anders, Pyl, & Huber, 2015) with the intersection-non-empty mode and counting ambiguous reads if fully overlapping. Raw counts were then normalized to fragments per kilobase of exon per million fragments mapped (FPKM) expression values.

Cell Culture and *In Vitro* Cytokine Stimulation

Human melanoma cell lines (M series) were established from patient's biopsies under UCLA IRB approval #11–003254 and human melanoma cell line 3998mel was provided by Alena Gros (Gros et al., 2016). Cells were cultured in RPMI 1640 with L-glutamine (Mediatech), 10% fetal bovine serum (Omega Scientific), and 1% penicillin-streptomycin (Omega Scientific) and were incubated in a water-saturated incubator at 37°C with 5% CO2. Cell lines were periodically authenticated to their early passages using GenePrint® 10 System (Promega).

Human recombinant IFNγ (Milipore Sigma) and human recombinant TNF (Peprotech) were each reconstituted in molecular grade water to 0.5 mg/ml and diluted in 0.1% BSA in PBS to 0.1 mg/ml before applying to cell culture media. The cytokines were stored in -80°C.

For *in vitro* long-term IFNγ experiments, cell lines were expanded and seeded onto 10cm tissue culture-treated plates at 70% confluency. After 24 hours to allow the cells to adhere

to the plates, new cell culture media containing 500 U/mL of human recombinant IFNγ protein were added. The cells were replenished with IFNγ-containing media every 2-3 days. Cells were seeded into multiple tissue culture plates and treated concurrently, so that a plate of cells could be harvested to perform flow cytometry each week without perturbing the rest of the cells and their ongoing exposure to interferon-gamma. For *in vitro* TNF experiments, the dose and time duration of exposure were kept same as the previously reported study (Landsberg et al., 2012) to use as positive control. Therefore, media containing 1000 U/mL of human recombinant TNF were added to plates of seeded cells and kept unperturbed for three days until the cells were harvested for downstream experiments.

Flow Cytometry

Cells were trypsinized, washed with PBS, and pelleted by centrifuging at 4°C for 5 minutes at 1500 RPM. All subsequent steps were performed with the cells on ice. Zombie Violet Fixable Viability Kit (BioLegend) was used per manufacturer's instructions. Next, cells were incubated in fetal bovine serum for 10 minutes to block unspecific binding. Cells were then incubated with anti-NGFR (PE) antibody (BioLegend) in PBS for 20 minutes. Following a wash, Cytofix/Cytoperm Fixation and Permeabilization Solution (BD Biosciences) was used per manufacturer's instructions to allow for the subsequent intracellular MART1 staining. All subsequent wash steps were performed using 1X Perm/Wash Buffer (BD Biosciences). Cells were incubated with anti-MART1 (Alexa Fluor 647) antibody (Santa Cruz Biotechnology) for 20 minutes and washed. OneComp eBeads compensation beads (ThermoFisher) were used for compensation. The samples were

run on the FACSCelesta Flow Cytometer (BD Biosciences), and the data were analyzed using the FlowJo software (TreeStar, Inc.).

RNA-Sequencing

RNA extraction was performed using the AllPrep DNA/RNA Mini Kit (Qiagen). Library preparation was performed by the Technology Center for Genomics & Bioinformatics (TCGB) at UCLA. RNA was sequenced on the HiSeq 3000 Sequencing System (Illumina) for a single-end 50 base run. Data quality was checked on Sequencing Analysis Viewer software (Illumina), and demultiplexing was performed using the bcl2fastq2 Conversion Software v2.17 (Illumina). Raw FASTQ data files were aligned to the hg19 genome using HISAT2 v2.0.4 with default parameters and counted using HTSeq v0.6.1. The raw counts were normalized to fragments per kilobase of exon per million fragments mapped (FPKM). DESeq2 was used to perform differential gene expression analysis.

Omni-ATAC Library Preparation and Sequencing

Cultured cells were harvested by trypsinization and were checked for viability of greater than 90%. After the cells were counted, 50,000 cells were resuspended in 1 ml of cold ATAC-seq resuspension buffer (RSB; 10 mM Tris-HCl pH 7.4, 10 mM NaCl, and 3 mM MgCl2 in water). Cells were centrifuged at 500 RCF for 5 min at 4°C in a fixed-angle centrifuge. Supernatant was carefully removed using two-step pipetting to avoid the cell pellet. Cell pellets were then resuspended in 50 µl of ATAC-seq RSB containing 0.1% NP40, 0.1% Tween-20, and 0.01% digitonin by pipetting up and down three times. This cell lysis reaction was incubated on ice for 3-5 min, with the lysis time optimized for each

sample. After lysis, 1 ml of ATAC-seq RSB containing 0.1% Tween-20 was added, and the tubes were inverted to mix. Nuclei were then centrifuged for 10 min at 500 RCF at 4°C in a fixed-angle centrifuge. Supernatant was carefully removed with two-step pipetting, and the nuclei were resuspended in 50 µl of transposition mix, which consisted of 25 µl of 2x TD buffer, 2.5 µl transposase (Illumina Nextera DNA Library Prep Kit), with 16.5 µl PBS, 0.5 µl 1% digitonin, 0.5 µl 10% Tween-20, and 5 µl water. Transposition reactions were incubated at 37°C for 1 hour in a thermomixer with shaking at 800 RPM. Reactions were cleaned up with Zymo DNA Clean and Concentrator columns and eluted in 10ul of nuclease-free water.

Following purification, the transposed DNA fragments were amplified using 1x NEBnext PCR Master Mix (New England BioLabs) and 1.25 µM of the Ad1_noMX primer and of the indexing primer (Buenrostro et al., 2013) in nuclease-free water for a 50ul reaction, with the following PCR conditions: 72 °C for 5 min; 98 °C for 30 s; and thermocycling at 98 °C for 10 s, 63 °C for 30 s and 72 °C for 1 min, for five cycles. To reduce GC content and size bias, qPCR was performed to determine the appropriate amount of amplification before saturation. To do this, 5 uL aliquot of the PCR reaction was added to 10 µl of the above PCR cocktail with the final concentration of 0.6x of SYBR Green (Thermo Fisher). The qPCR cycle was run at 98 °C for 30 s followed by 20 cycles of 98 °C for 10 s, 63 °C for 30 s, and 72 °C for 1 min to determine the additional number of cycles needed for the remaining 45 µL reaction. The libraries were purified using a Qiagen MinElute PCR Purification Kit. All libraries met the target concentration of 20 µl at 4 nM, determined by the Qubit Fluorometric Quantitation (Thermo Fisher).

Sequencing was performed on the NextSeq 500 (Illumina) for a paired-end 75 base run, and at least 50 million paired reads were obtained for each sample.

Omni-ATAC Data Processing

The raw FASTQ files were processed using the published ENCODE ATAC-seq Pipeline (https://github.com/kundajelab/atac_dnase_pipelines). The reads were trimmed and aligned to hg38 using bowtie2. Picard was used to de-duplicate reads, which were then filtered for high quality, paired reads using samtools. All peak calling was performed using macs2. The optimal Irreproducible Discovery Rate (IDR) thresholded peak output was used for all downstream analyses, with a threshold p-value of 0.05. Other ENCODE3 parameters were enforced with the flag --encode3. Reads that mapped to mitochondrial genes or blacklisted regions, as defined by the ENCODE pipeline, were removed. The peak files were merged using bedtools merge to create a consensus set of peaks across all samples, and the number of reads in each peak was determined using bedtools multicov (Quinlan & Hall, 2010). DESeq2 with default parameters was used to normalize read counts (Love, Huber, & Anders, 2014) and to determine the the hyperaccessible and hypoaccessible peaks following cytokine exposure. Peaks were called as hyper- or hypo-accessible using abs (log2 fold change)>0.5 and adjusted $p<0.05$.

PCA/PLSR and projections

Log2 transformed fragments per kilobase per million (FPKM) of coding genes was used to perform unsupervised principal component analysis (PCA). This method uncovers

latent components which are linear combinations of the features that most strongly vary across the datasets. PCA was performed centered and unscaled using the *prcomp* function in R. Projections onto PCA frameworks were done using custom script by multiplication of the original projected sample scores by the PCA rotation matrix. PCA of ATACseq data was performed centered and unscaled using normalized counts of the union of all significantly induced peaks. Partial Least Squares Regression (PLSR) is a supervised version of PCA that seeks to find the latent vectors that maximize the covariance of the input variables (e.g. gene expression) and the response (e.g. phenotypes). Varimax rotation of the PLSR loadings ($PLSR_v$) was performed on 2 components, without Kaiser normalization and using the R package *varimax*, in order to simplify the structure of the loading matrix.

Mutation Analysis

The patient-derived human melanoma cell lines were sequenced and characterized for their mutational status as previously described (Atefi et al., 2014; Nazarian et al., 2010; Wong et al., 2014).

Gene Set Enrichment Analysis and Gene Ontology

Gene Set Enrichment Analysis (GSEA) (Subramanian et al., 2005) and GSEA-squared was done on pre-ranked lists of genes using the MSigDB C5 gene sets and Kolmogorov-Smirnov (KS) statistics. GSEA-squared was performed as previously described (Balanis et al., 2019) . Briefly, all individual words in the genesets were collected and their frequencies were tabulated. Words with frequencies <5 or >500 were excluded, and all

gene sets were then ranked by their NES value. Keywords and their categories were further assigned by manual curation of the top of the ranked list of words.

Rank Rank Hypergeometric Overlap (RRHO)

Rank Rank Hypergeometric Overlap was performed for gene expression data by taking the rank of varimax-rotated PLSR loadings, and calculating the hypergeometric p-values of the TNF-d0 versus IFNγ-d0 ranked lists using the online tool and the R package RRHO. RRHO for genesets was performed after running GSEA on ranked gene lists, and ranking gene sets by their Normalized Enrichment Score. Step size 100 was used for genes and gene sets (Plaisier et al., 2010).

Motif Enrichment Analysis

Differential peak analysis was first conducted using DESeq2 on normalized ATACseq counts. Starting from the full consensus peak set, samples were divided into baseline differentiated and baseline undifferentiated groups, and hypo- and hyper-accessible peaks were called separately for TNF vs d0, and IFNγ vs d0, at adjusted p-value < 0.05 and log2 fold-change >2, without independent filtering or Cook's cutoff. Motif analysis was done on each of these peak sets using HOMER against a whole genome background and searching for motifs within +/-200bp from the peak center. Raw -ln(p-values) were plotted for TNF-induced vs IFNγ-induced hyper accessible motifs. Overlap of significantly differential peaks was calculated and plotted as Venn diagrams using the R package *Vennerable*.

ARACNe and VIPER Analysis

ARACNe (Lachmann, Giorgi, Lopez, & Califano, 2016) network connections were created using all genes, and then the network nodes were restricted to transcription factors (TFs) by combining all TF gene sets in the GO gene ontology. A single network was built using melanoma RNAseq samples from the M-series cohort (Grasso et al., under review). VIPER analysis (Alvarez et al., 2016) was performed using the R *msviper* function from the package viper, with a minimum network size of 10.

Figure 1.

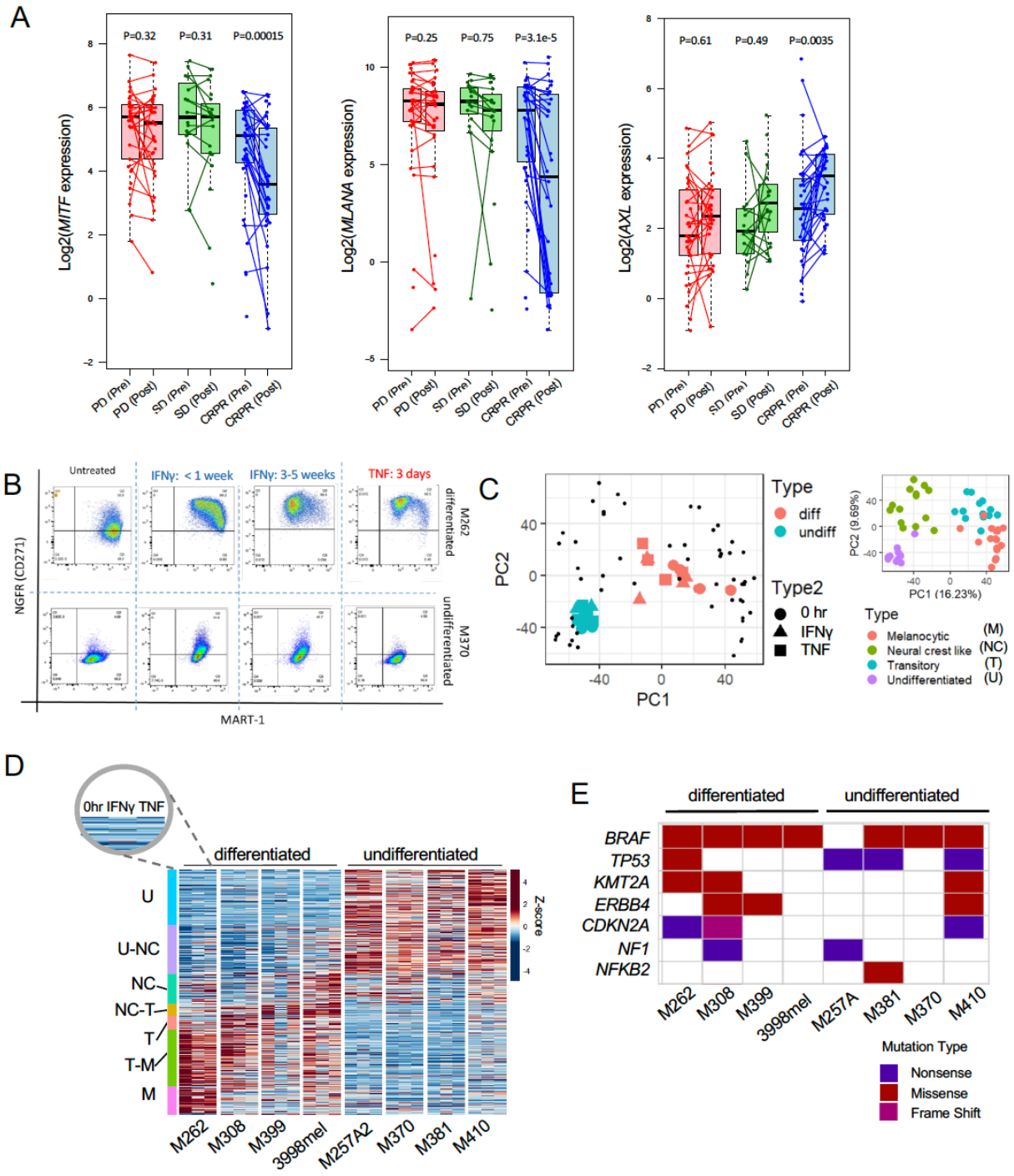
A
P=0.32
P=0.31
P=0.00015
Log2(MITF expression)
P=0.25
P=0.75
P=3.1e-5
Log2(MLANA expression)
P=0.61
P=0.49
P=0.0035
Log2(AXL expression)
PD (Pre)
PD (Post)
SD (Pre)
SD (Post)
CRPR (Pre)
CRPR (Post)
B
Untreated
IFNγ: < 1 week
IFNγ: 3-5 weeks
TNF: 3 days
M262
differentiated
M370
undifferentiated
NGFR (CD271)
MART-1
C
Type
diff
undiff
Type2
0 hr
IFNγ
TNF
PC1
PC2
PC1 (16.23%)
PC2 (9.69%)
Type
Melanocytic (M)
Neural crest like (NC)
Transitory (T)
Undifferentiated (U)
D
0hr IFNγ TNF
differentiated
undifferentiated
U
U-NC
NC
NC-T
T
T-M
M
Z-score
M262
M308
M399
3998mel
M257A2
M370
M381
M410
E
differentiated
undifferentiated
BRAF
TP53
KMT2A
ERBB4
CDKN2A
NF1
NFKB2
M262
M308
M399
3998mel
M257A
M381
M370
M410
Mutation Type
Nonsense
Missense
Frame Shift

Figure 2.

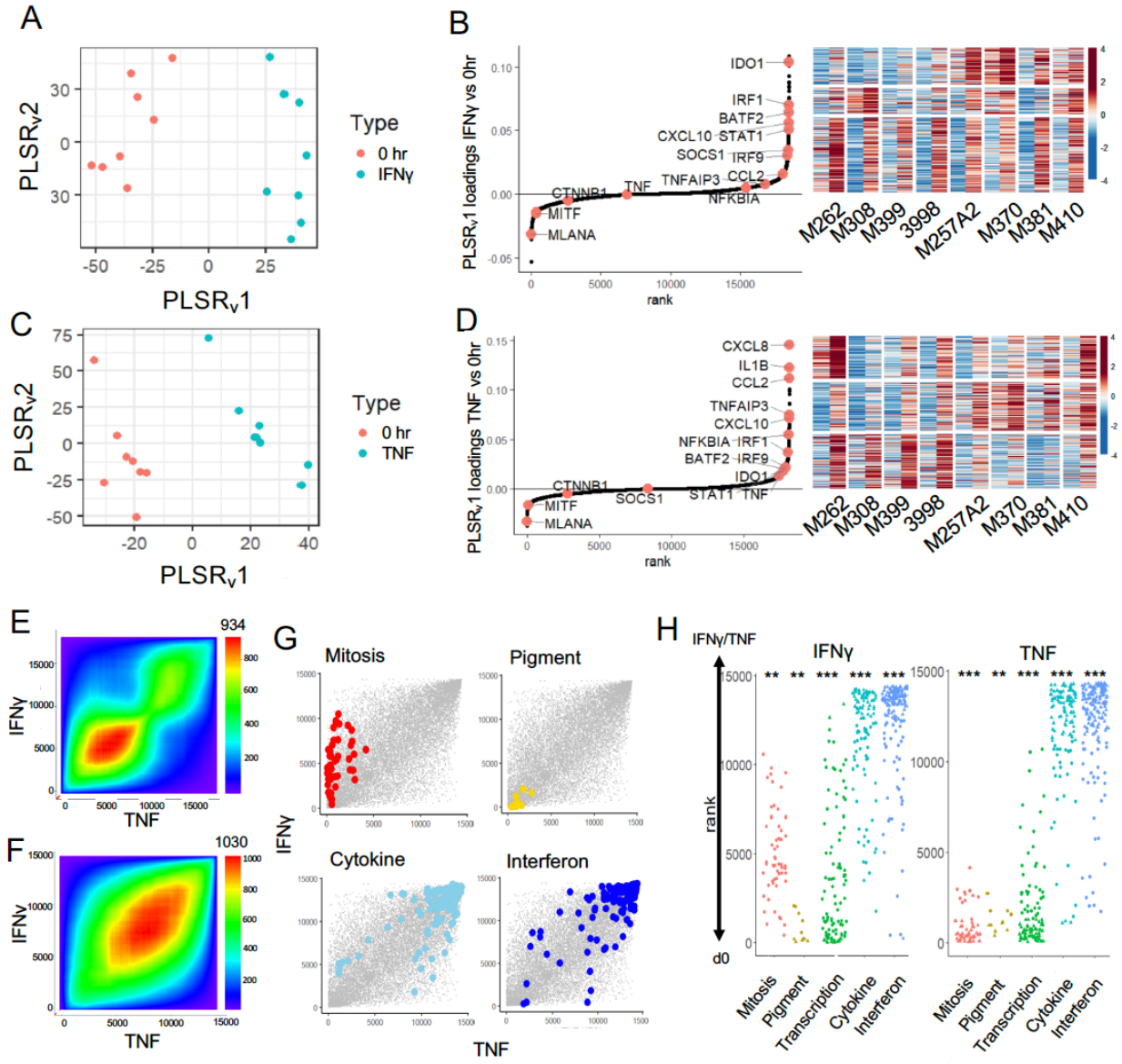
A
PLSRv2
PLSRv1
Type
0 hr
IFNγ
B
PLSRv1 loadings IFNγ vs 0hr
rank
IDO1
IRF1
BATF2
CXCL10
STAT1
SOCS1
IRF9
TNFAIP3
CCL2
NFKBIA
TNF
CTNNB1
MITF
MLANA
M262
M308
M399
3998
M257A2
M370
M381
M410
C
PLSRv2
PLSRv1
Type
0 hr
TNF
D
PLSRv1 loadings TNF vs 0hr
rank
CXCL8
IL1B
CCL2
TNFAIP3
CXCL10
NFKBIA
IRF1
BATF2
IRF9
IDO1
STAT1
TNF
SOCS1
CTNNB1
MITF
MLANA
E
934
IFNγ
TNF
F
1030
IFNγ
TNF
G
Mitosis
Pigment
Cytokine
Interferon
IFNγ
TNF
H
IFNγ/TNF
IFNγ
TNF
rank
d0
Mitosis
Pigment
Transcription
Cytokine
Interferon

Figure 3.

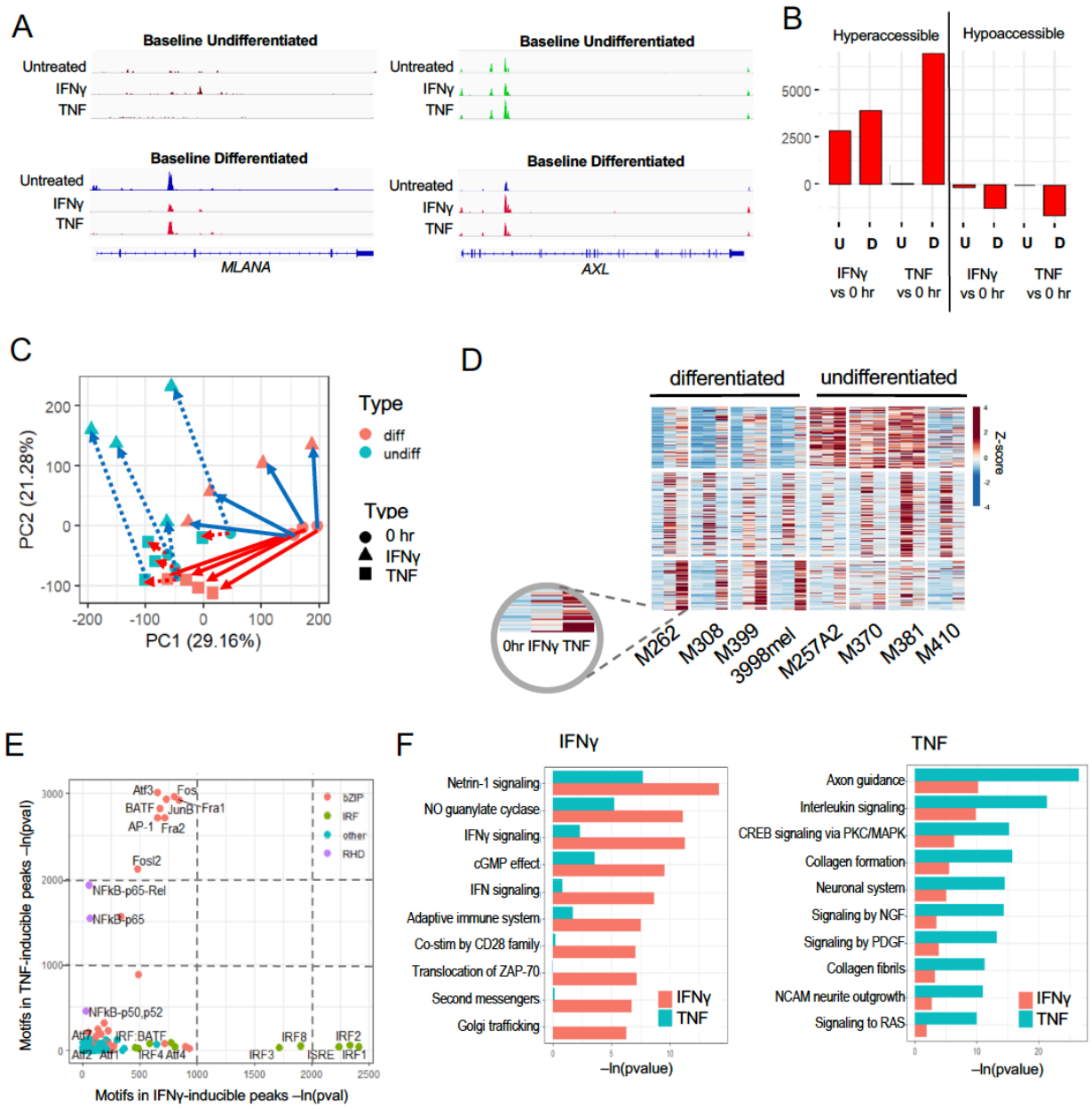
A
Baseline Undifferentiated
Untreated
IFNγ
TNF
Baseline Differentiated
MLANA
AXL
B
Hyperaccessible
Hypoaccessible
5000
2500
0
U D U D U D U D
IFNγ vs 0 hr
TNF vs 0 hr
C
PC2 (21.28%)
PC1 (29.16%)
Type
diff
undiff
Type
0 hr
IFNγ
TNF
D
differentiated
undifferentiated
Z-score
0hr IFNγ TNF
M262
M308
M399
3998mel
M257A2
M370
M381
M410
E
Motifs in TNF-inducible peaks –ln(pval)
Motifs in IFNγ-inducible peaks –ln(pval)
bZIP
IRF
other
RHD
Atf3
Fos
BATF
JunB
Fra1
AP-1
Fra2
Fosl2
NFkB-p65-Rel
NFkB-p65
NFkB-p50,p52
IRF:BATF
Atf7
Atf2
Atf1
IRF4
Atf4
IRF3
IRF8
ISRE
IRF2
IRF1
F
IFNγ
Netrin-1 signaling
NO guanylate cyclase
IFNγ signaling
cGMP effect
IFN signaling
Adaptive immune system
Co-stim by CD28 family
Translocation of ZAP-70
Second messengers
Golgi trafficking
–ln(pvalue)
TNF
Axon guidance
Interleukin signaling
CREB signaling via PKC/MAPK
Collagen formation
Neuronal system
Signaling by NGF
Signaling by PDGF
Collagen fibrils
NCAM neurite outgrowth
Signaling to RAS
–ln(pvalue)

Figure 4.

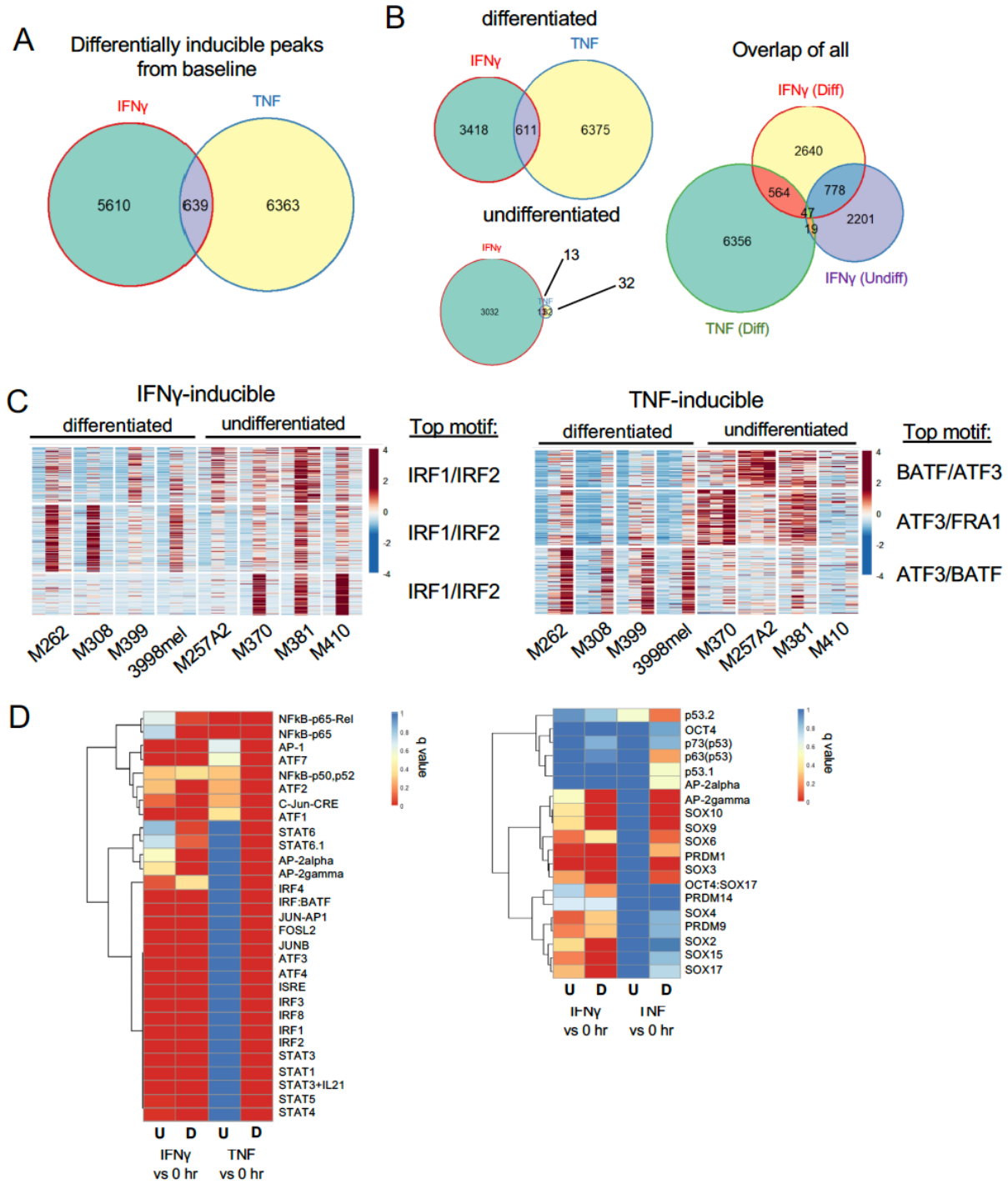
A
Differentially inducible peaks from baseline
IFNγ
TNF
5610
639
6363
B
differentiated
IFNγ
TNF
3418
611
6375
undifferentiated
IFNγ
3032
13
32
Overlap of all
IFNγ (Diff)
2640
564
778
47
19
2201
6356
IFNγ (Undiff)
TNF (Diff)
C
IFNγ-inducible
differentiated
undifferentiated
Top motif:
IRF1/IRF2
IRF1/IRF2
IRF1/IRF2
M262
M308
M399
3998mel
M257A2
M370
M381
M410
TNF-inducible
differentiated
undifferentiated
Top motif:
BATF/ATF3
ATF3/FRA1
ATF3/BATF
M262
M308
M399
3998mel
M370
M257A2
M381
M410
D
NFkB-p65-Rel
NFkB-p65
AP-1
ATF7
NFkB-p50,p52
ATF2
C-Jun-CRE
ATF1
STAT6
STAT6.1
AP-2alpha
AP-2gamma
IRF4
IRF:BATF
JUN-AP1
FOSL2
JUNB
ATF3
ATF4
ISRE
IRF3
IRF8
IRF1
IRF2
STAT3
STAT1
STAT3+IL21
STAT5
STAT4
q value
U D U D
IFNγ vs 0 hr
TNF vs 0 hr
p53.2
OCT4
p73(p53)
p63(p53)
p53.1
AP-2alpha
AP-2gamma
SOX10
SOX9
SOX6
PRDM1
SOX3
OCT4:SOX17
PRDM14
SOX4
PRDM9
SOX2
SOX15
SOX17
q value
U D U D
IFNγ vs 0 hr
TNF vs 0 hr

Figure 5.

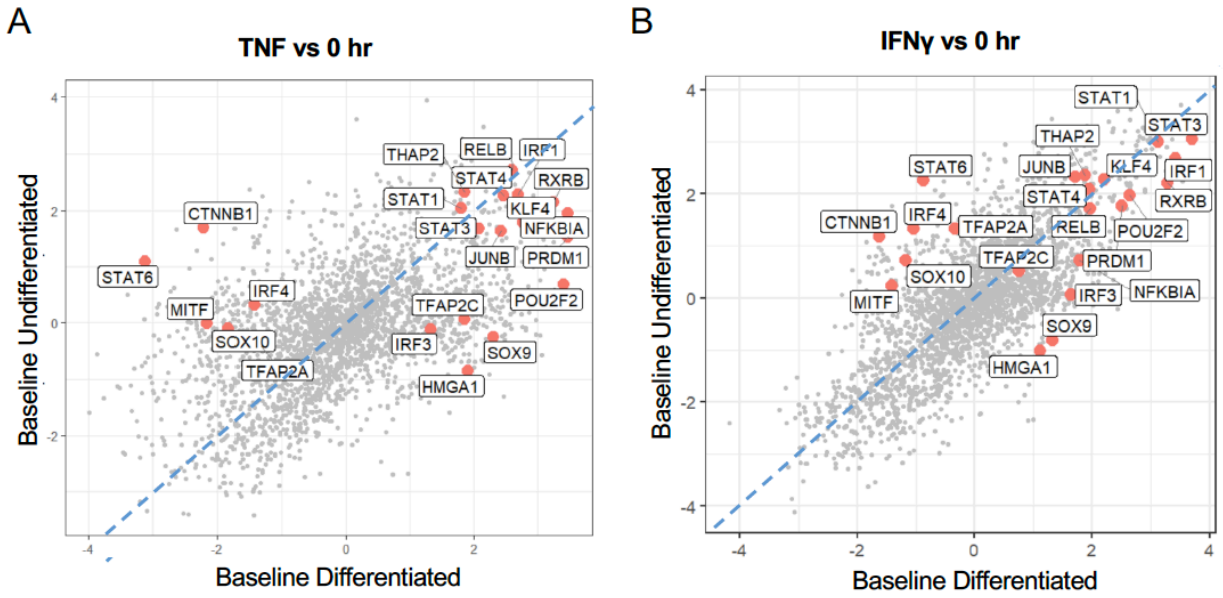
A
TNF vs 0 hr
Baseline Undifferentiated
Baseline Differentiated
THAP2
RELB
IRF1
STAT4
RXRB
STAT1
KLF4
CTNNB1
STAT3
NFKBIA
JUNB
PRDM1
STAT6
IRF4
MITF
TFAP2C
POU2F2
SOX10
IRF3
SOX9
TFAP2A
HMGA1
B
IFNγ vs 0 hr
Baseline Undifferentiated
Baseline Differentiated
STAT1
STAT3
THAP2
STAT6
JUNB
KLF4
IRF1
STAT4
RXRB
CTNNB1
IRF4
TFAP2A
RELB
POU2F2
TFAP2C
PRDM1
SOX10
MITF
IRF3
NFKBIA
SOX9
HMGA1

Figure 6.

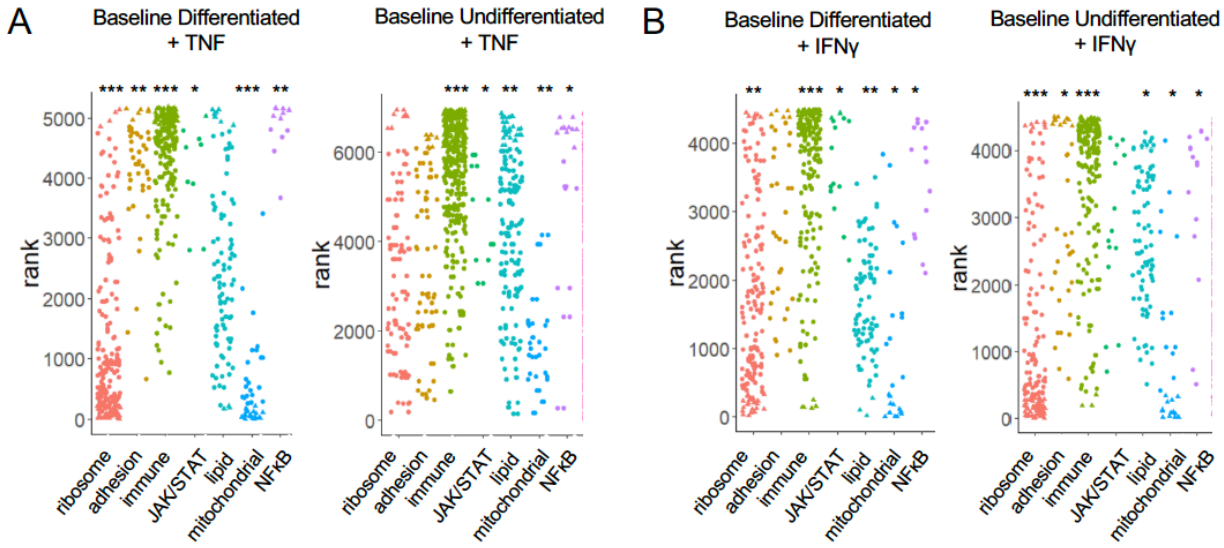
A
Baseline Differentiated
+ TNF
Baseline Undifferentiated
+ TNF
B
Baseline Differentiated
+ IFNγ
Baseline Undifferentiated
+ IFNγ
rank
ribosome
adhesion
immune
JAK/STAT
lipid
mitochondrial
NFκB

Figure 7.

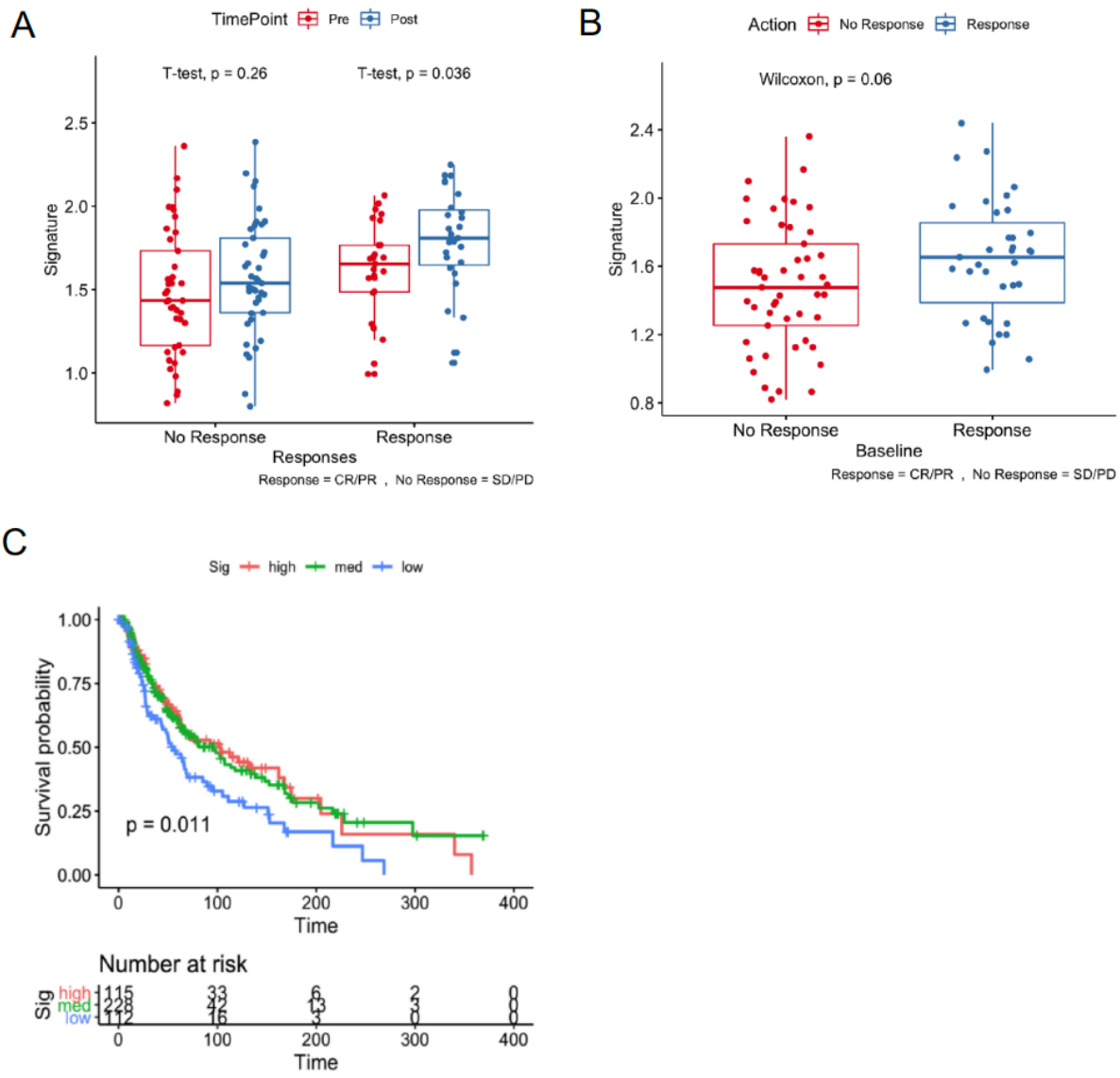
A
TimePoint Pre Post
T-test, p = 0.26
T-test, p = 0.036
Signature
No Response
Response
Responses
Response = CR/PR , No Response = SD/PD
B
Action No Response Response
Wilcoxon, p = 0.06
Signature
No Response
Response
Baseline
Response = CR/PR , No Response = SD/PD
C
Sig high med low
Survival probability
p = 0.011
Time
Number at risk
Sig
high 115 33 6 2 0
med 228 42 13 3 0
low 112 16 3 0 0
Time

Figure S1.

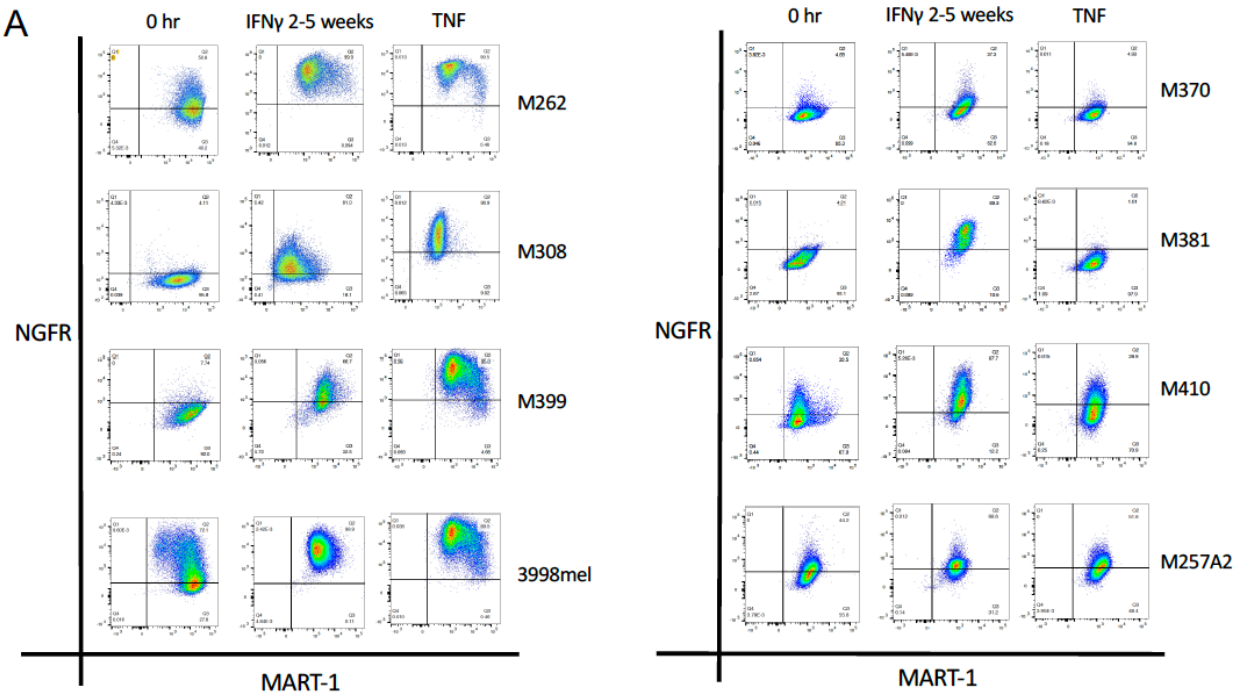
A
0 hr
IFNγ 2-5 weeks
TNF
M262
M308
M399
3998mel
NGFR
MART-1
M370
M381
M410
M257A2

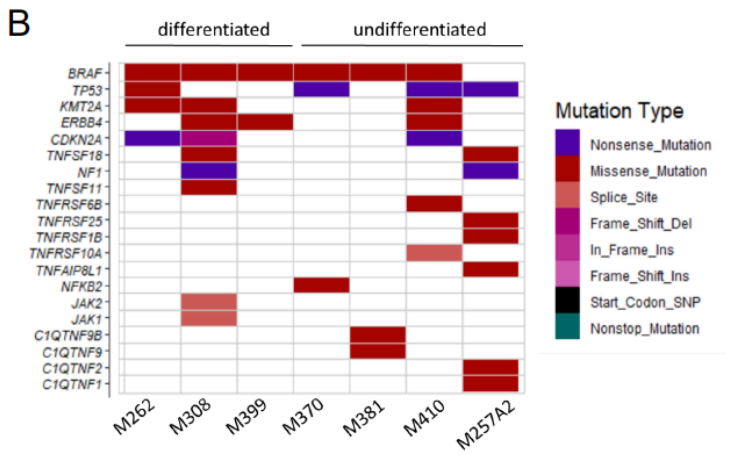
B
differentiated
undifferentiated
BRAF
TP53
KMT2A
ERBB4
CDKN2A
TNFSF18
NF1
TNFSF11
TNFRSF6B
TNFRSF25
TNFRSF1B
TNFRSF10A
TNFAIP8L1
NFKB2
JAK2
JAK1
C1QTNF9B
C1QTNF9
C1QTNF2
C1QTNF1
M262
M308
M399
M370
M381
M410
M257A2
Mutation Type
Nonsense_Mutation
Missense_Mutation
Splice_Site
Frame_Shift_Del
In_Frame_Ins
Frame_Shift_Ins
Start_Codon_SNP
Nonstop_Mutation

Figure S2.

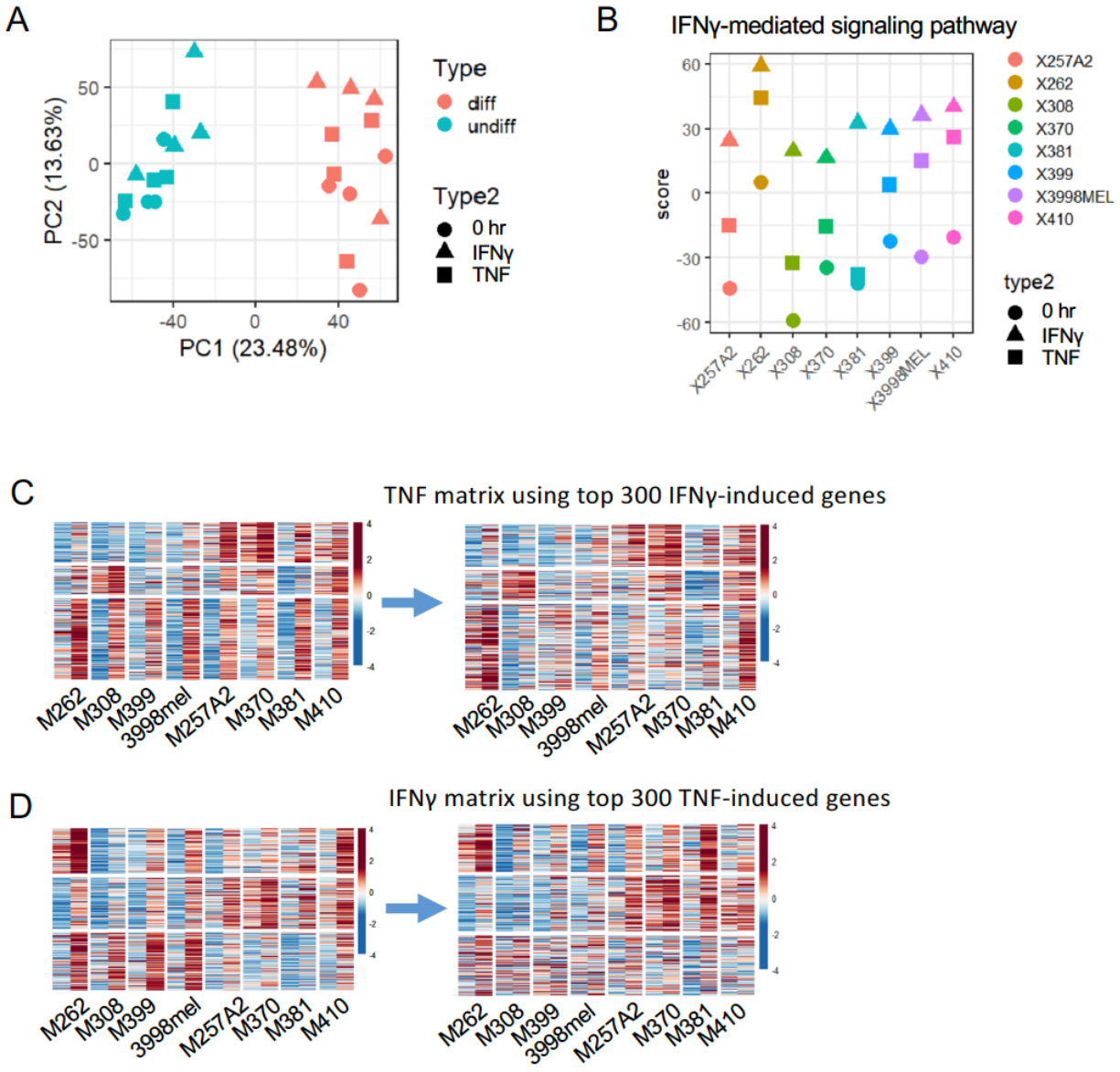
A
PC2 (13.63%)
PC1 (23.48%)
Type
diff
undiff
Type2
0 hr
IFNγ
TNF
B
IFNγ-mediated signaling pathway
score
X257A2
X262
X308
X370
X381
X399
X3998MEL
X410
type2
0 hr
IFNγ
TNF
C
TNF matrix using top 300 IFNγ-induced genes
M262
M308
M399
3998mel
M257A2
M370
M381
M410
D
IFNγ matrix using top 300 TNF-induced genes

Figure S3.

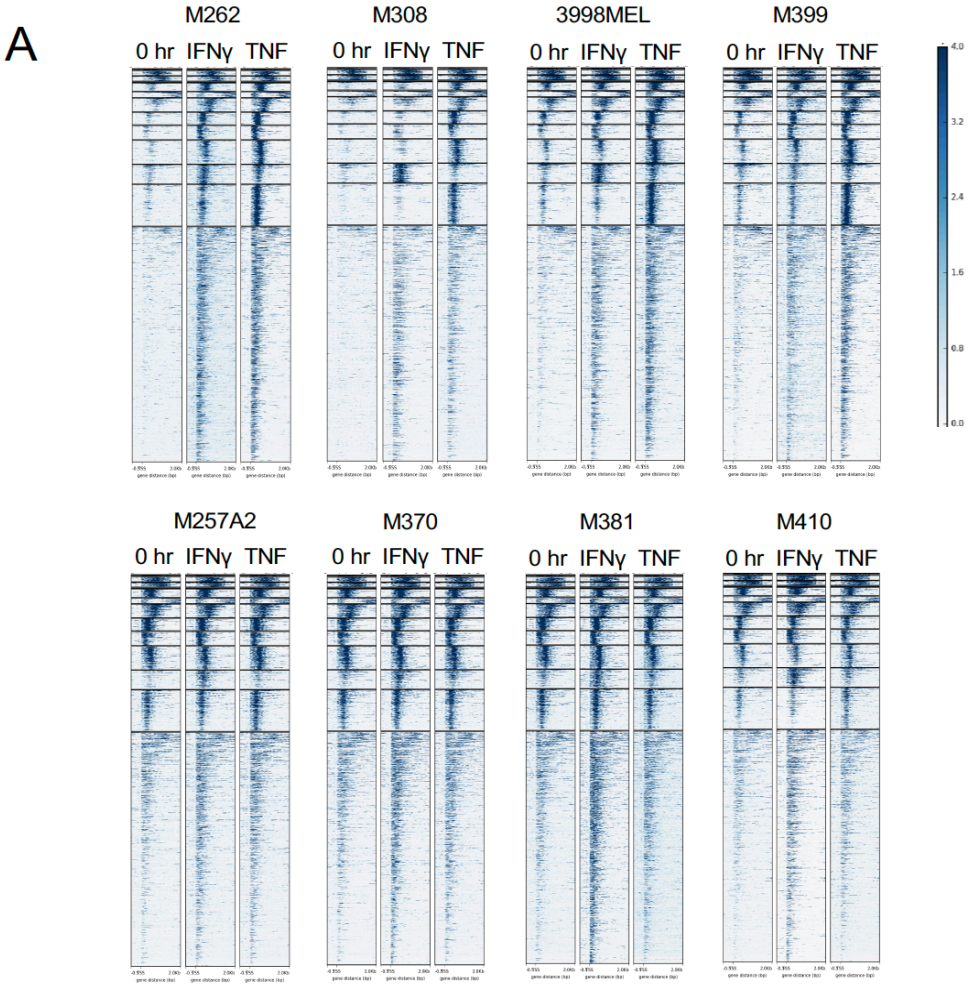
A
M262
M308
3998MEL
M399
M257A2
M370
M381
M410
0 hr IFNγ TNF
4.0
3.2
2.4
1.6
0.8
0.0

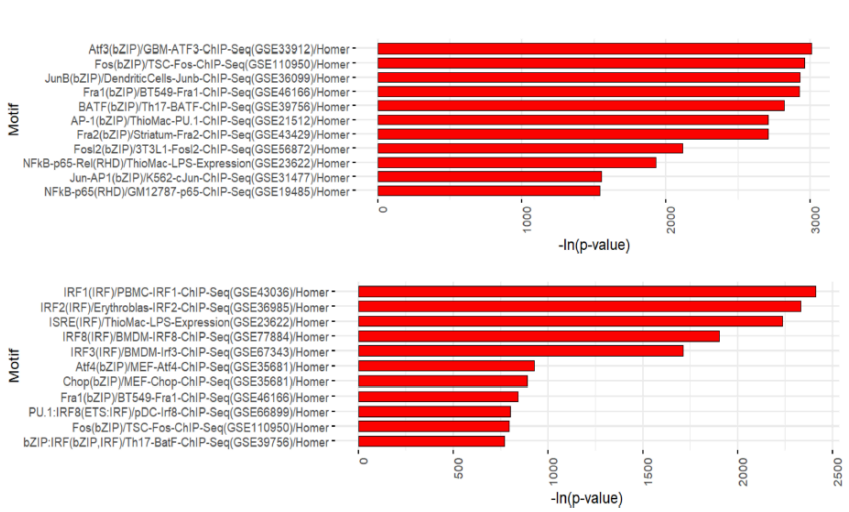
B
Motif
Atf3(bZIP)/GBM-ATF3-ChIP-Seq(GSE33912)/Homer
Fos(bZIP)/TSC-Fos-ChIP-Seq(GSE110950)/Homer
JunB(bZIP)/DendriticCells-Junb-ChIP-Seq(GSE36099)/Homer
Fra1(bZIP)/BT549-Fra1-ChIP-Seq(GSE46166)/Homer
BATF(bZIP)/Th17-BATF-ChIP-Seq(GSE39756)/Homer
AP-1(bZIP)/ThioMac-PU.1-ChIP-Seq(GSE21512)/Homer
Fra2(bZIP)/Striatum-Fra2-ChIP-Seq(GSE43429)/Homer
Fosl2(bZIP)/3T3L1-Fosl2-ChIP-Seq(GSE56872)/Homer
NFkB-p65-Rel(RHD)/ThioMac-LPS-Expression(GSE23622)/Homer
Jun-AP1(bZIP)/K562-cJun-ChIP-Seq(GSE31477)/Homer
NFkB-p65(RHD)/GM12787-p65-ChIP-Seq(GSE19485)/Homer
0
1000
2000
3000
-ln(p-value)
Motif
IRF1(IRF)/PBMC-IRF1-ChIP-Seq(GSE43036)/Homer
IRF2(IRF)/Erythroblas-IRF2-ChIP-Seq(GSE36985)/Homer
ISRE(IRF)/ThioMac-LPS-Expression(GSE23622)/Homer
IRF8(IRF)/BMDM-IRF8-ChIP-Seq(GSE77884)/Homer
IRF3(IRF)/BMDM-Irf3-ChIP-Seq(GSE67343)/Homer
Atf4(bZIP)/MEF-Atf4-ChIP-Seq(GSE35681)/Homer
Chop(bZIP)/MEF-Chop-ChIP-Seq(GSE35681)/Homer
Fra1(bZIP)/BT549-Fra1-ChIP-Seq(GSE46166)/Homer
PU.1:IRF8(ETS:IRF)/pDC-Irf8-ChIP-Seq(GSE66899)/Homer
Fos(bZIP)/TSC-Fos-ChIP-Seq(GSE110950)/Homer
bZIP:IRF(bZIP,IRF)/Th17-BatF-ChIP-Seq(GSE39756)/Homer
0
500
1000
1500
2000
2500
-ln(p-value)

Figure S4.

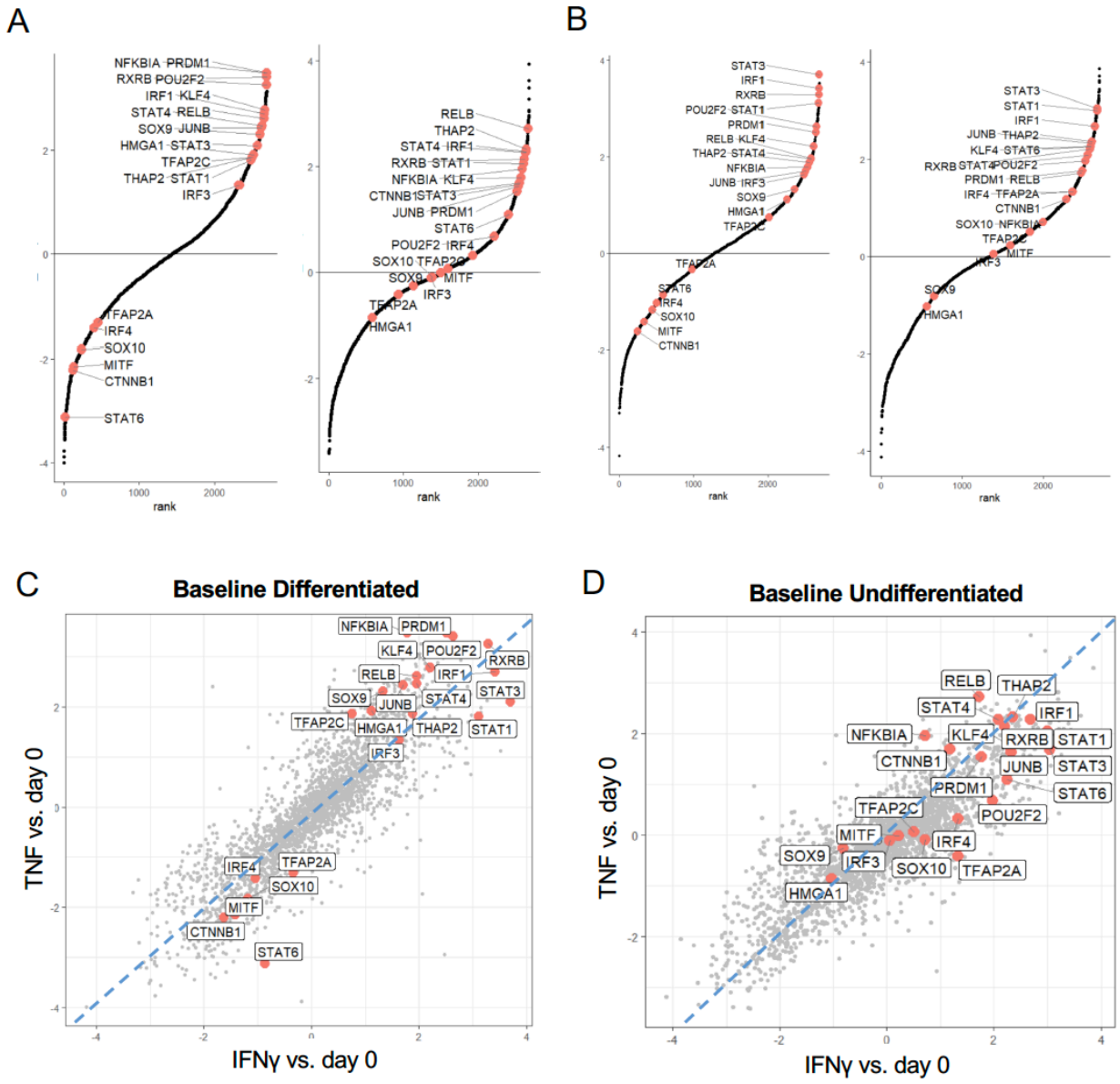
A
NFKBIA PRDM1
RXRB POU2F2
IRF1 KLF4
STAT4 RELB
SOX9 JUNB
HMGA1 STAT3
TFAP2C
THAP2 STAT1
IRF3
TFAP2A
IRF4
SOX10
MITF
CTNNB1
STAT6
RELB
THAP2
STAT4 IRF1
RXRB STAT1
NFKBIA KLF4
CTNNB1 STAT3
JUNB PRDM1
STAT6
POU2F2 IRF4
SOX10 TFAP2C
SOX9 MITF
IRF3
TFAP2A
HMGA1
rank
B
STAT3
IRF1
RXRB
POU2F2 STAT1
PRDM1
RELB KLF4
THAP2 STAT4
NFKBIA
JUNB IRF3
SOX9
HMGA1
TFAP2C
TFAP2A
STAT6
IRF4
SOX10
MITF
CTNNB1
STAT3
STAT1
IRF1
JUNB THAP2
KLF4 STAT6
RXRB STAT4 POU2F2
PRDM1 RELB
IRF4 TFAP2A
CTNNB1
SOX10 NFKBIA
TFAP2C
MITF
IRF3
SOX9
HMGA1
rank
C
Baseline Differentiated
NFKBIA PRDM1
KLF4 POU2F2
RXRB
RELB IRF1
SOX9 JUNB STAT4
STAT3
TFAP2C HMGA1 THAP2 STAT1
IRF3
IRF4 TFAP2A
SOX10
MITF
CTNNB1
STAT6
TNF vs. day 0
IFNγ vs. day 0
D
Baseline Undifferentiated
RELB THAP2
STAT4
IRF1
NFKBIA KLF4 RXRB STAT1
CTNNB1
JUNB STAT3
PRDM1
STAT6
TFAP2C
POU2F2
MITF
IRF4
SOX9
IRF3
SOX10 TFAP2A
HMGA1
TNF vs. day 0
IFNγ vs. day 0

References

Alvarez, M. J., Shen, Y., Giorgi, F. M., Lachmann, A., Ding, B. B., Hilda Ye, B., & Califano, A. (2016). Functional characterization of somatic mutations in cancer using network-based inference of protein activity. *Nature Genetics*, *48*(8), 838–847. https://doi.org/10.1038/ng.3593

Anders, S., Pyl, P. T., & Huber, W. (2015). HTSeq--a Python framework to work with high-throughput sequencing data. *Bioinformatics*, *31*(2), 166–169. https://doi.org/10.1093/bioinformatics/btu638

Atefi, M., Avramis, E., Lassen, A., Wong, D. J. L., Robert, L., Foulad, D., … Ribas, A. (2014). Effects of MAPK and PI3K Pathways on PD-L1 Expression in Melanoma. *Clinical Cancer Research*, *20*(13), 3446–3457. https://doi.org/10.1158/1078-0432.CCR-13-2797

Ayers, M., Lunceford, J., Nebozhyn, M., Murphy, E., Loboda, A., Kaufman, D. R., … McClanahan, T. K. (2017). IFN-γ–related mRNA profile predicts clinical response to PD-1 blockade. *The Journal of Clinical Investigation*, *127*(8), 2930–2940. https://doi.org/10.1172/JCI91190

Balanis, N. G., Sheu, K. M., Esedebe, F. N., Patel, S. J., Smith, B. A., Park, J. W., … Graeber, T. G. (2019). Pan-cancer Convergence to a Small-Cell Neuroendocrine Phenotype that Shares Susceptibilities with Hematological Malignancies. *Cancer Cell*, *36*(1), 17-34.e7. https://doi.org/10.1016/J.CCELL.2019.06.005

Bellei, B., Pitisci, A., Catricalà, C., Larue, L., & Picardo, M. (2011). Wnt/β-catenin signaling is stimulated by α-melanocyte-stimulating hormone in melanoma and

melanocyte cells: implication in cell differentiation. *Pigment Cell & Melanoma Research*, *24*(2), 309–325. https://doi.org/10.1111/j.1755-148X.2010.00800.x

Cristescu, R., Mogg, R., Ayers, M., Albright, A., Murphy, E., Yearley, J., … Kaufman, D. (2018). Pan-tumor genomic biomarkers for PD-1 checkpoint blockade–based immunotherapy. *Science*, *362*(6411), eaar3593. https://doi.org/10.1126/science.aar3593

Falletta, P., Sanchez-del-Campo, L., Chauhan, J., Effern, M., Kenyon, A., Kershaw, C. J., … Goding, C. R. (2017). Translation reprogramming is an evolutionarily conserved driver of phenotypic plasticity and therapeutic resistance in melanoma. *Genes & Development*. https://doi.org/10.1101/GAD.290940.116

Gros, A., Parkhurst, M. R., Tran, E., Pasetto, A., Robbins, P. F., Ilyas, S., … Rosenberg, S. A. (2016). Prospective identification of neoantigen-specific lymphocytes in the peripheral blood of melanoma patients. *Nature Medicine*, *22*(4), 433–438. https://doi.org/10.1038/nm.4051

Hoek, K. S., Schlegel, N. C., Eichhoff, O. M., Widmer, D. S., Praetorius, C., Einarsson, S. O., … Steingrimsson, E. (2008). Novel MITF targets identified using a two-step DNA microarray strategy. *Pigment Cell & Melanoma Research*, *21*(6), 665–676. https://doi.org/10.1111/j.1755-148X.2008.00505.x

Hölzel, M., & Tüting, T. (2016). Inflammation-Induced Plasticity in Melanoma Therapy and Metastasis. *Trends in Immunology*, *37*(6), 364–374. https://doi.org/10.1016/j.it.2016.03.009

Kim, D., Paggi, J. M., Park, C., Bennett, C., & Salzberg, S. L. (2019). Graph-based genome alignment and genotyping with HISAT2 and HISAT-genotype. *Nature*

Biotechnology, *37*(8), 907–915. https://doi.org/10.1038/s41587-019-0201-4

Konieczkowski, D. J., Johannessen, C. M., Abudayyeh, O., Kim, J. W., Cooper, Z. A., Piris, A., … Garraway, L. A. (2014). A Melanoma Cell State Distinction Influences Sensitivity to MAPK Pathway Inhibitors. *Cancer Discovery*, *4*(7), 816–827. https://doi.org/10.1158/2159-8290.CD-13-0424

Lachmann, A., Giorgi, F. M., Lopez, G., & Califano, A. (2016). ARACNe-AP: gene network reverse engineering through adaptive partitioning inference of mutual information. *Bioinformatics*, *32*(14), 2233–2235. https://doi.org/10.1093/bioinformatics/btw216

Landsberg, J., Kohlmeyer, J., Renn, M., Bald, T., Rogava, M., Cron, M., … Tüting, T. (2012). Melanomas resist T-cell therapy through inflammation-induced reversible dedifferentiation. *Nature*, *490*(7420), 412–416. https://doi.org/10.1038/nature11538

Love, M. I., Huber, W., & Anders, S. (2014). Moderated estimation of fold change and dispersion for RNA-seq data with DESeq2. *Genome Biology*, *15*(12), 550. https://doi.org/10.1186/s13059-014-0550-8

Mehta, A., Kim, Y. J., Robert, L., Tsoi, J., Comin-Anduix, B., Berent-Maoz, B., … Ribas, A. (2018). Immunotherapy resistance by inflammation-induced dedifferentiation. *Cancer Discovery*, *8*(8), 935–943. https://doi.org/10.1158/2159-8290. CD-17-1178

Müller, J., Krijgsman, O., Tsoi, J., Robert, L., Hugo, W., Song, C., … Peeper, D. S. (2014). Low MITF/AXL ratio predicts early resistance to multiple targeted drugs in melanoma. *Nature Communications*, *5*(1), 5712. https://doi.org/10.1038/ncomms6712

Nazarian, R., Shi, H., Wang, Q., Kong, X., Koya, R. C., Lee, H., … Lo, R. S. (2010). Melanomas acquire resistance to B-RAF(V600E) inhibition by RTK or N-RAS upregulation. *Nature*, *468*(7326), 973–977. https://doi.org/10.1038/nature09626

Opdecamp, K., Nakayama, A., Nguyen, M. T. T., Hodgkinson, C. A., Pavan, W. J., & Arnheiter, H. (1997). Melanocyte development in vivo and in neural crest cell cultures: Crucial dependence on the Mitf basic-helix-loop-helix-zipper transcription factor. *Development*, *124*(12), 2377–2386.

Plaisier, S. B., Taschereau, R., Wong, J. A., & Graeber, T. G. (2010). Rank–rank hypergeometric overlap: identification of statistically significant overlap between gene-expression signatures. *Nucleic Acids Research*, *38*(17), e169–e169. https://doi.org/10.1093/nar/gkq636

Quinlan, A. R., & Hall, I. M. (2010). BEDTools: a flexible suite of utilities for comparing genomic features. *Bioinformatics*, *26*(6), 841–842. https://doi.org/10.1093/bioinformatics/btq033

Rambow, F., Rogiers, A., Marin-Bejar, O., Aibar, S., Femel, J., Dewaele, M., … Marine, J.-C. (2018). Toward Minimal Residual Disease-Directed Therapy in Melanoma. *Cell*, *174*(4), 843-855.e19. https://doi.org/10.1016/j.cell.2018.06.025

Restivo, G., Diener, J., Cheng, P. F., Kiowski, G., Bonalli, M., Biedermann, T., … Sommer, L. (2017). The low affinity neurotrophin receptor CD271 regulates phenotype switching in melanoma. *Nature Communications*, *8*(1), 1988. https://doi.org/10.1038/s41467-017-01573-6

Riaz, N., Havel, J. J., Makarov, V., Desrichard, A., Urba, W. J., Sims, J. S., … Chan, T. A. (2017). Tumor and Microenvironment Evolution during Immunotherapy with

Nivolumab. *Cell*, *171*(4), 934-949.e16. https://doi.org/10.1016/j.cell.2017.09.028

Ribas, A., & Wolchok, J. D. (2018). Cancer immunotherapy using checkpoint blockade. *Science*, *359*(6382), 1350–1355. https://doi.org/10.1126/science.aar4060

Riesenberg, S., Groetchen, A., Siddaway, R., Bald, T., Reinhardt, J., Smorra, D., … Hölzel, M. (2015). MITF and c-Jun antagonism interconnects melanoma dedifferentiation with pro-inflammatory cytokine responsiveness and myeloid cell recruitment. *Nature Communications*, *6*. https://doi.org/10.1038/NCOMMS9755

Shin, D. S., Zaretsky, J. M., Escuin-Ordinas, H., Garcia-Diaz, A., Hu-Lieskovan, S., Kalbasi, A., … Ribas, A. (2017). Primary Resistance to PD-1 Blockade Mediated by JAK1/2 Mutations. *Cancer Discovery*. https://doi.org/10.1158/2159-8290.CD-16-1223

Subramanian, A., Tamayo, P., Mootha, V. K., Mukherjee, S., Ebert, B. L., Gillette, M. A., … Mesirov, J. P. (2005). Gene set enrichment analysis: A knowledge-based approach for interpreting genome-wide expression profiles. *Proceedings of the National Academy of Sciences*, *102*(43), 15545–15550. https://doi.org/10.1073/PNAS.0506580102

Tachibana, M., Takeda, K., Nobukuni, Y., Urabe, K., Long, J. E., Meyers, K. A., … Miki, T. (1996). Ectopic expression of MITF, a gene for Waardenburg syndrome type 2, converts fibroblasts to cells with melanocyte characteristics. *Nature Genetics*, *14*(1), 50–54. https://doi.org/10.1038/ng0996-50

Tirosh, I., Izar, B., Prakadan, S. M., Wadsworth, M. H., Treacy, D., Trombetta, J. J., … Garraway, L. A. (2016). Dissecting the multicellular ecosystem of metastatic melanoma by single-cell RNA-seq. *Science (New York, N.Y.)*, *352*(6282), 189–196.

https://doi.org/10.1126/science.aad0501

Tsoi, J., Robert, L., Paraiso, K., Galvan, C., Sheu, K. M., Lay, J., … Graeber, T. G. (2018). Multi-stage Differentiation Defines Melanoma Subtypes with Differential Vulnerability to Drug-Induced Iron-Dependent Oxidative Stress. *Cancer Cell*, *33*(5), 890-904.e5. https://doi.org/10.1016/j.ccell.2018.03.017

Tumeh, P. C., Harview, C. L., Yearley, J. H., Shintaku, I. P., Taylor, E. J. M., Robert, L., … Ribas, A. (2014). PD-1 blockade induces responses by inhibiting adaptive immune resistance. *Nature*, *515*(7528), 568. https://doi.org/10.1038/NATURE13954

Wong, D. J., Robert, L., Atefi, M. S., Lassen, A., Avarappatt, G., Cerniglia, M., … Ribas, A. (2014). Antitumor activity of the ERK inhibitor SCH722984 against BRAF mutant, NRAS mutant and wild-type melanoma. *Molecular Cancer*, *13*(1), 194. https://doi.org/10.1186/1476-4598-13-194

Yang, L., Wei, Y., Sun, Y., Shi, W., Yang, J., Zhu, L., & Li, M. (2015). Interferon-gamma inhibits melanogenesis and induces apoptosis in melanocytes: A pivotal role of CD8+ cytotoxic T lymphocytes in vitiligo. *Acta Dermato-Venereologica*, *95*(6), 664–670. https://doi.org/10.2340/00015555-2080

Yoshida, H., Kunisada, T., Kusakabe, M., Nishikawa, S., Nishikawa, S. I., Bartlett, P. F., & Murphy, M. (1996). Distinct stages of melanocyte differentiation revealed by anlaysis of nonuniform pigmentation patterns. *Development (Cambridge, England)*, *122*(4), 1207–1214. Retrieved from http://www.ncbi.nlm.nih.gov/pubmed/8620847

Zaretsky, J. M., Garcia-Diaz, A., Shin, D. S., Escuin-Ordinas, H., Hugo, W., Hu-Lieskovan, S., … Ribas, A. (2016). Mutations Associated with Acquired Resistance to PD-1 Blockade in Melanoma. *New England Journal of Medicine*, *375*(9), 819–

829. https://doi.org/10.1056/NEJMoa1604958